How Drugs Interact with Transporters: SGLT1 as a Model

**Donald D. F. Loo · Bruce A. Hirayama ·
Monica Sala-Rabanal · Ernest M. Wright**

Abstract Drugs are transported by cotransporters with widely different turnover rates. We have examined the underlying mechanism using, as a model system, glucose and indican (indoxyl-β-D-glucopyranoside) transport by human Na$^+$/glucose cotransporter (hSGLT1). Indican is transported by hSGLT1 at 10% of the rate for glucose but with a fivefold higher apparent affinity. We expressed wild-type hSGLT1 and mutant G507C in *Xenopus* oocytes and used electrical and optical methods to measure the kinetics of glucose (using nonmetabolized glucose analogue α-methyl-D-glucopyranoside, αMDG) and indican transport, alone and together. Indican behaved as a competitive inhibitor of αMDG transport. To examine protein conformations, we recorded SGLT1 capacitive currents (charge movements) and fluorescence changes in response to step jumps in membrane voltage, in the presence and absence of indican and/or αMDG. In the absence of sugar, voltage jumps elicited capacitive SGLT currents that decayed to steady state with time constants (τ) of 3–20 ms. These transient currents were abolished in saturating αMDG but only slightly reduced (10%) in saturating indican. SGLT1 G507C rhodamine fluorescence intensity increased with depolarizing and decreased with hyperpolarizing voltages. Maximal fluorescence increased $\sim$150% in saturating indican but decreased $\sim$50% in saturating αMDG. Modeling indicated that the rate-limiting step for indican transport is sugar translocation, whereas for αMDG it is dissociation of Na$^+$ from the internal binding sites. The inhibitory effects of indican on αMDG transport are due to its higher affinity and a 100-fold lower translocation rate. Our results indicate that competition between substrates and drugs should be taken into consideration when targeting transporters as drug delivery systems.

Keywords Na$^+$/glucose cotransport turnover · Competitive inhibition of sugar transport · Drug–cotransporter interactions · Steady-state and pre-steady-state kinetics · Fluorescence · Conformational change

Introduction

Cotransporters are membrane proteins that use energy stored in the transmembrane electrochemical gradient of ions (Na$^+$ or protons) to drive transport of substrates against their concentration gradient, enabling the efficient accumulation of substrate in the cell. Many have been found to transport a wide variety of substrate analogues, and in recent years there has been increasing interest in using them as vehicles for drug delivery. We and others have shown that substrate analogues are transported at widely different turnover rates. For example, in the glucose (human Na$^+$/glucose cotransporter 1 [hSGLT1], pig SGLT3), nucleoside (hCNT1, hCNT3, NUpC) and dipeptide (hPEPT1, hPEPT2) cotransporters drugs are transported at maximum rates varying from 10% to 150% of that for the natural substrates (Lostao et al. 1994; Díez-Sampedro et al. 2000; Veyhl et al. 1998; Loewen et al. 2004; Knutter et al. 2007; Sala-Rabanal et al. 2006; Larrayoz et al. 2004; Smith et al. 2004; King et al. 2006). An unanswered question, mechanistically and pharmacologically, is why substrate analogues have different turnover rates.

D. D. F. Loo (✉) · B. A. Hirayama · M. Sala-Rabanal ·
E. M. Wright
Department of Physiology, David Geffen School of Medicine
at UCLA, 10833 LeConte Avenue, Los Angeles,
CA 90095-1751, USA
e-mail: dloo@mednet.ucla.edu
URL: http//140.142.237.182/

From a functional point of view, one of the most extensively studied transporters is SGLT1. Secondary active sugar transport occurs by an alternating access mechanism via a series of conformational changes induced by ligand (Na$^+$ and glucose) binding and membrane voltage (Fig. 1) (Parent et al. 1992; Loo et al. 2002, 2006; Hirayama et al. 2007). In the normal transport cycle, two external Na$^+$ ions bind to the empty (ligand-free) transporter and cause a conformational change that results in an increase in affinity for glucose. Sugar binding induces a conformational change of the fully loaded transporter to expose the ligand-binding sites to the internal membrane surface, where glucose is released into the cytoplasm before the Na$^+$ ions. The empty transporter then returns to the external membrane surface. External Na$^+$ binding/ dissociation and reorientation of the ligand-free binding sites between faces of the membrane are voltage-dependent.

In this study, we examined the mechanism underlying the transport of substrates with different turnover rates using glucose and indican (indoxyl-β-D-glucopyranoside) transport by hSGLT1 as a model system. Indican is transported at 10% of the maximal rate of glucose but with a 10-fold greater apparent affinity—half-maximal concentration ($K_{0.5}$) is 80 μM for indican vs. 300 μM for glucose (Díez-Sampedro et al. 2000). We expressed wild-type hSGLT1 and mutant G507C in *Xenopus laevis* oocytes and used electrical and fluorescence measurements to study the steady-state and pre-steady-state kinetics in the presence of indican and/or α-methyl-D-glucopyranoside (αMDG). These latter measurements allowed us to monitor the conformational states of the transporter during sugar transport.

The rate-limiting step for transport of natural substrates (glucose and galactose) is the internal release of Na$^+$ from SGLT1 (Loo et al. 2006). In contrast, we found that the rate-limiting step for indican transport is translocation across the membrane, i.e., the conformational change of the fully loaded (Na$^+$ and indican bound) protein from the outward-facing to the inward-facing conformation. Physiologically, the differences in binding and membrane translocation rates between indican and glucose lead to competition between the two sugars, resulting in inhibition of glucose transport by indican. Since other cotransporters also transport drugs with very different turnover rates, we predict that competition between drugs and natural substrates could have a significant effect when cotransporters are targeted as drug delivery systems. It is also clear that identification of the transport step affected will aid in drug design as the "binding pharmacophore" is distinct from the "transport pharmacophore."
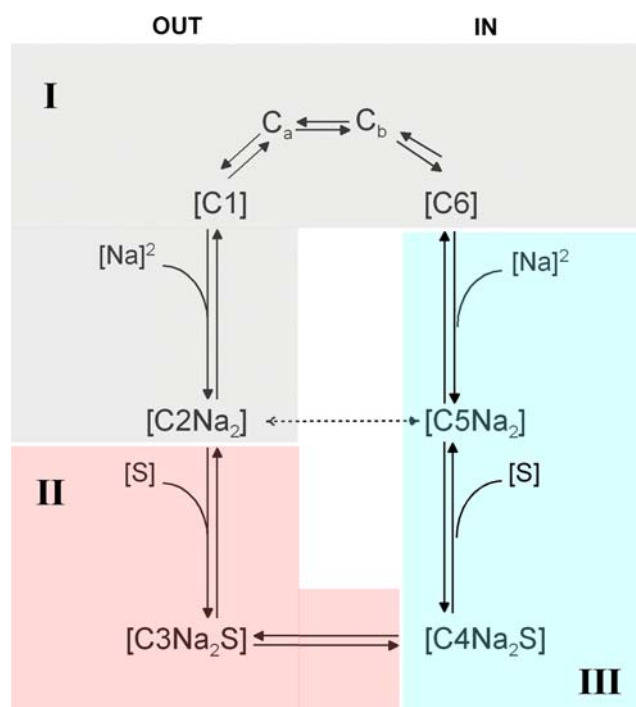

Fig. 1 Eight-state ordered kinetic model for Na$^+$/glucose transport by SGLT1 (from Loo et al. 2006). Kinetic states of the transporter are the empty transporter (C_1, C_6), Na$^+$-bound (C2Na$_2$, C5Na$_2$) and Na$^+$- and sugar-bound (C3Na$_2$S, C$_4$Na$_2$S) in the external and internal membrane surfaces. Two Na$^+$ ions bind to the protein before the sugar molecule. The partial reactions fall into three groups: *I* (gray region), voltage-dependent reactions—these are the conformational changes of the empty transporter between external and internal membrane surfaces ($C_1 \rightleftarrows C_a \rightleftarrows C_b \rightleftarrows C_6$) and Na$^+$ binding/ dissociation ($C_1 \rightleftarrows$ C2Na$_2$); *II* (red region), external sugar binding/ dissociation (C2Na$_2 \rightleftarrows$ C3Na$_2$S) and sugar translocation across the cell membrane (C3Na$_2$S $\rightleftarrows$ C4Na$_2$S); and *III* (blue region), internal Na$^+$ release (C5Na$_2 \rightarrow C_6$) and sugar release (C4Na$_2$S $\rightarrow$ C5Na$_2$). *Dashed line* between C2Na$_2$ and C5Na$_2$ is the uniport mode of Na$^+$ transport by SGLT1. In this study experiments were conducted under conditions close to zero-trans, i.e., internal [sugar] = 0 mM, internal [Na$^+$] = 5 mM

Materials and Methods

Preparation and Maintenance of Oocytes

Mature *X. laevis* oocytes were isolated, defolliculated, injected with wild-type hSGLT1 or hSGLT1 mutant G507C cRNA (see Loo et al. 1993, 1998, 2006). hSGLT1 G507C-expressing oocytes were completely labeled with tetramethylrhodamine-6-maleimide (TMR6M; Invitrogen Molecular Probes, Carlsbad, CA) (Loo et al. 1998, 2006; Meinild et al. 2002). After labeling, oocytes were washed free of dye and kept in NaCl buffer in the dark until use. Oocytes were bathed in NaCl buffer containing (mM) 100 NaCl, 2 KCl, 1 CaCl$_2$, 1 MgCl$_2$ and 10 HEPES (pH 7.4). αMDG or indican was added to the superfusing NaCl buffer at the reported concentrations.

Combined Electrophysiological and Fluorescence Experiments

Electrophysiological and simultaneous electrophysiological and fluorescence experiments were performed on hSGLT1 and TMR6M-labeled hSGLT1 G507C, as described previously (Loo et al. 1998, 2006; Meinild et al. 2002). The TMR6M-labeled mutant transporter exhibited similar kinetics as wild-type hSGLT1, before and after labeling of Cys507 by TMR6M (Loo et al. 2006). A standard pulse protocol was applied where membrane potential was held at -50 mV (V_h) and stepped to various test values (V_t from $+90$ to -150 mV in 20-mV decrements) for 100 or 300 ms before returning to V_h. The current records were the averages of three sweeps (Loo et al. 2006). Records were filtered at 500 or 150 Hz, depending on the sampling interval (0.1 or 0.3 ms per sample). In the present study, we did not record the fast components of charge movement and rhodamine fluorescence intensity change (ΔF) observed previously using cut-open oocyte voltage-clamp fluorometry (Loo et al. 2005). Fluorescence intensity is expressed as arbitrary units (au). For oocytes expressing mutant G507C labeled with TMR6M and bathed in NaCl buffer, $\Delta F_{max}/F_{total}$ is $\approx 1\%$ (ΔF_{max} is the maximal fluorescence intensity change and F_{total} is total fluorescence intensity). Fluorescence data have been corrected for photobleaching and rundown (Meinild et al. 2002). All experiments were performed at room temperature (20–23°C).

Data Analysis

Steady-State Currents

To obtain the current–voltage (I–V) relations of sugar- (αMDG and indican) induced currents, a protocol with voltage pulses of 100–300 ms was applied. The sugar-induced current was the difference between the currents at the end of the pulse in the presence of external sugar from baseline in NaCl buffer. Sugar-induced currents (at each voltage) were fitted to:

$$I = I_{max} ([S]_o)^n / \{ (K0.5)^n + ([S]_o)^n \} \quad (1)$$

where I_{max} is the maximal sugar-induced current, $[S]_o$ is the external Na$^+$ or sugar concentration, $K_{0.5}$ is the half-maximal concentration ($[S]_o$ at 50% I_{max}) and n is the Hill coefficient. For sugar activation n is 1, and for Na$^+$ n is 2 (Birnir et al. 1991; Parent et al. 1992; Mackenzie et al. 1998; Loo et al. 2006). The sugar- (αMDG) induced cotransporter current is directly proportional to the Na$^+$ and sugar uptake into the cell, with a stoichiometry of 2Na$^+$/1αMDG (Mackenzie et al. 1998; Quick et al. 2001).

Isolation of Pre-Steady-State Currents

In response to a voltage pulse, the total membrane current is composed of the bilayer capacitive transient, pre-steady-state SGLT1 currents and steady-state currents. In the absence of sugar, steady-state currents consisted of background endogenous currents of the oocyte and Na$^+$ leak (uniporter mode) of SGLT1 (Parent et al. 1992; Loo et al. 1998). Total membrane current (I_{tot}) was fitted to:

$$I_{tot}(t) = I_{cm} \exp(-t/\tau_{cm}) + I_{med} \exp(-t/\tau_{med}) + I_{slow} \exp(-t/\tau_{slow}) + I_{ss} \quad (2)$$

where I_{ss} is the steady-state current and $I_{cm} \exp(-t/\tau_{cm})$ is the bilayer capacitance current, with initial value I_{cm} and time constant τ_{cm}. $I_{med} \exp(-t/\tau_{med})$ and $I_{slow} \exp(-t/\tau_{slow})$ are the medium and slow components of SGLT1 pre-steady-state current with initial values (I_{med}, I_{slow}) and time constants (τ_{med}, τ_{slow}). The SGLT1 pre-steady-state currents ($I_{med} \exp(-t/\tau_{med}) + I_{slow} \exp(-t/\tau_{slow})$) were isolated as described previously (Loo et al. 2005). SGLT1 charge movement (Q) was obtained from the integral of the SGLT1 pre-steady-state currents. Steady-state current (I_{ss}) consisted of oocyte background current, Na$^+$-uniporter current (of SGLT1) and Na$^+$/sugar cotransport current. The cotransport current was taken as the difference in the steady-state current recorded in the presence and absence of substrate.

The time course of total fluoresence intensity change (ΔF_{total}) was also fitted to two exponential components: $\Delta F_{total} = \Delta F_{med} (1 - \exp(-t/\tau_{med}) + \Delta F_{slow} (1 - \exp(-t/\tau_{slow})$, where ΔF_{med}, ΔF_{slow}, τ_{med} and τ_{slow} are the amplitude and time constants of the medium and slow components (Loo et al. 2005, 2006).

Fitting of $Q-V$ and $\Delta F-V$ relations

The charge vs. voltage ($Q-V$) relations could, to a first approximation, be fitted with a single Boltzmann function (Loo et al. 1993, 2005; Hazama et al. 1997):

$$(Q - Q_{hyp})/Q_{max} = 1/[1 + \exp(z\delta(V - V_{0.5})F/RT] \quad (3)$$

where Q_{max} is the maximal charge ($Q_{dep} - Q_{hyp}$), Q_{dep} and Q_{hyp} are the Q (absolute value) at depolarizing and hyperpolarizing limits, V is membrane potential, F is Faraday constant, R is gas constant, T is absolute temperature, $V_{0.5}$ is midpoint voltage (membrane potential at 50% Q_{max}) and $z\delta$ is maximum steepness factor for the dependence of Q on voltage or apparent valence of the voltage sensor. $z\delta$ is the product of the apparent valence of the movable charge (z) and the fraction of the membrane electric field traversed by the charge (δ). For Q_{hyp} to be the limit at large hyperpolarizing voltages (equation 3), we assume $z < 0$.

We denote $z\delta^Q$ and $V_{0.5}^Q$ for the $(z\delta)$ and $V_{0.5}$ obtained from charge measurements.

The Boltzmann relation was also used to empirically fit the $\Delta F_{total} - V$ curves (Loo et al. 2006), with Q_{dep}, Q_{hyp} and Q_{max} replaced by ΔF_{dep}, ΔF_{hyp} and ΔF_{max}, respectively. Parameters obtained were maximal fluorescence intensity change ($\Delta F_{max} = \Delta F_{dep} - \Delta F_{hyp}$), membrane voltage at 50% ΔF_{max} ($V_{0.5}^F$) and apparent valence or voltage-steepness factor for fluorescence ($z\delta^F$).

Fits of data to equations were performed using either Sigmaplot 10 (SPSS, Inc., Chicago, IL) or Clampfit 10.1 (Axon Instruments, Union City, CA). For data obtained on a single oocyte, the statistics are given by the estimates and standard error of the fit. When data are from a population,

the statistics are given by the means and standard errors of the means with the number of samples. While data are shown for representative experiments, all experiments were performed on at least three oocytes from different batches.

Results

Steady-State Kinetics

Basic Electrical Characteristics

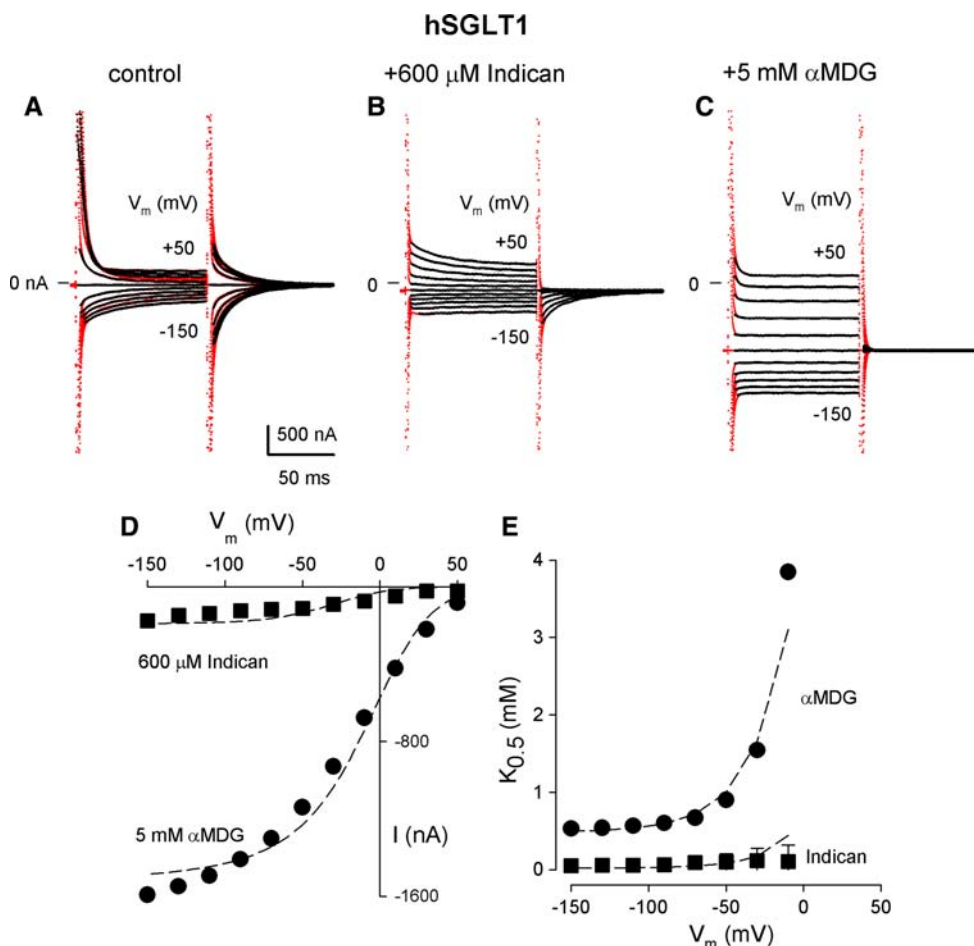Figure 2A shows the total current records from an oocyte expressing hSGLT1 in response to step jumps in membrane

Fig. 2 Current records from an oocyte expressing hSGLT1. Membrane potential was held at -50 mV (V_h), and a series of 100-ms test voltage pulses (V_t) was applied (from $+50$ to -150 mV in 20-mV decrements). *Red traces* represent total current and *black traces* are the records with the oocyte membrane capacitance subtracted using the fitted method (see "Materials and Methods"). (**A**) Current records in NaCl buffer alone. (**B**) In the presence of 600 μM indican. (**C**) In the presence of 5 mM αMDG. (**D**) I–V curves of the indican- and αMDG-induced steady-state currents. (**E**) Dependence of $K_{0.5}^{indican}$ and $K_{0.5}^{\alpha MDG}$ on membrane voltage. Note that at $+50$ mV the pre-steady-state current has not reached steady state at 100 ms; thus, the indican

cotransport current is slightly overestimated. *Dashed curves* in (**D**) and (**E**) were obtained by simulation of the model of Fig. 8 (equation 6 of Appendix). Values of the kinetic parameters used were within the range listed in Table 1: $k_{12} = 45,000$ M^{-2}s^{-1}, $k_{21} = 300$ s^{-1}, $k_{1a} = 600$ s^{-1}, $k_{a1} = 50$ s^{-1}, $k_{ab} = 5$ s^{-1}, $k_{ba} = 40$ s^{-1}, $k_{b6} = 100$ s^{-1}, $k_{6b} = 100$ s^{-1}, $k_{25} = 0.01$ s^{-1}, $k_{52} = 3.5$ x 10^{-4} s^{-1}, $k_{56} = 5$ s^{-1}, $k_{65} = 2,250$ M^{-2}s^{-1}, $k_{23} = 45,000$ M^{-1}s^{-1}, $k_{32} = 20$ s^{-1}, $k_{45} = 800$ s^{-1}, $k_{54} = 81,667$ M^{-1}s^{-1}, $k_{34} = 50$ s^{-1}, $k_{43} = 50$ s^{-1}, $k_{27} = 250,000$ M^{-1}s^{-1}, $k_{72} = 12$ s^{-1}, $k_{85} = 800$ s^{-1}, $k_{58} = 756,173$ M^{-1}s^{-1}, $k_{78} = 0.5$ s^{-1}, $k_{87} = 0.5$ s^{-1}. Total number of transporters $N_T = 1.5 \times 10^{12}$

voltage (from $+50$ to -150 mV) from the holding potential ($V_h = -50$ mV). External solution contained NaCl buffer free of sugar. After the initial capacitance transient of the oocyte membrane bilayer (time constant $\tau \approx 0.8$ ms, highlighted in red), the pre-steady-state current of hSGLT1 decayed to steady state with τ 3–20 ms (Loo et al. 1993, 2005, 2006; Quick et al. 2001). The steady-state current is composed of the Na$^+$ uniporter current (or Na$^+$ leak) of hSGLT1 and the endogenous background current of the oocyte (Parent et al. 1992; Loo et al. 1999).

There was an increase in steady-state current in the presence of indican (e.g., 600 μM, Fig. 2B) and αMDG (e.g., 5 mM, Fig. 2C). The sugar-induced current, obtained by subtracting the steady-state current in NaCl buffer from the total current in the presence of sugar, was much greater in αMDG than indican. The I–V relations of both sugars tended toward saturation at large hyperpolarizing voltages and approached zero-current in the depolarizing direction (Fig. 2D). For V_m between -50 and -150 mV, current induced by saturating concentrations of indican ($I_{max}^{indican}$) was $\approx 10\%$ of the maximal αMDG-induced current ($I_{max}^{\alpha MDG}$): e.g., at -50 mV, $I_{max}^{indican}$ and $I_{max}^{\alpha MDG}$ were 113 and 1,141 nA in one oocyte. The dashed curves are the predicted I–V curves obtained from simulation of the kinetic model for SGLT1 using the kinetic parameters for indican and αMDG (Table 1).

The $K_{0.5}$ for indican ($K_{0.5}^{Indican}$) varied from 97 to 51 μM for membrane voltages between -50 and -150 mV (Fig. 2E). In comparison, $K_{0.5}$ for αMDG ($K_{0.5}^{\alpha MDG}$) varied from 0.9 to 0.5 mM for V_m between -50 and -150 (Fig. 2E). The dashed curves are model predictions using the kinetic parameters for indican and αMDG (Table 1).

Cotransport in the Presence of αMDG and Indican

In the presence of αMDG, indican behaved as an inhibitor. This is illustrated by the I–V curves in Fig. 3A, which shows that the current induced by αMDG alone (0.25 mM, black circles) was reduced when indican (60 and 480 μM) was added to the external solution containing αMDG. The maximal current induced by saturating [indican]$_o$ in the presence of 0.25 mM αMDG approached the current induced by saturating indican alone (not shown). The reduction of sugar-induced current (obtained by subtracting the current induced by αMDG and indican together from the current induced by αMDG alone) with increasing [indican]$_o$ was dose-dependent and hyperbolic. At $V_m = -50$ mV, the apparent inhibitory constant (K_i) was 247 ± 84 μM ($n = 3$, Fig. 3B), higher than the $K_{0.5}$ for Na$^+$/indican cotransport alone (60 μM, Fig. 2E). The curve in Fig. 3B was predicted by the kinetic model (Fig. 8) with a K_i of
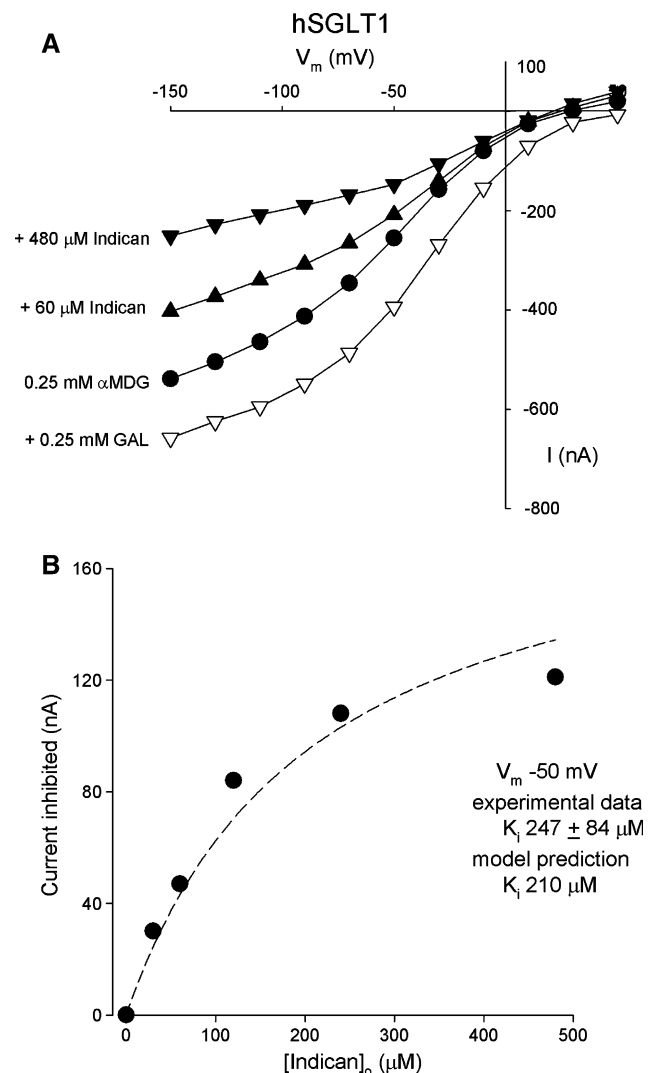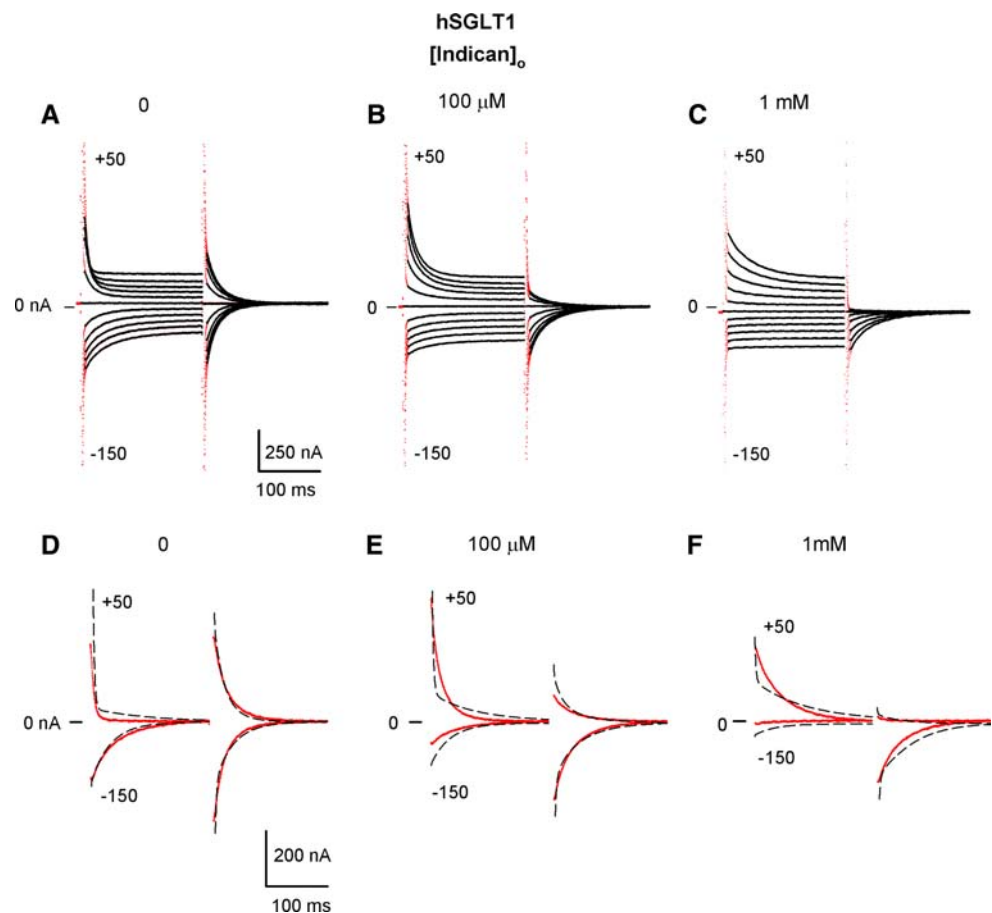

Fig. 3 Competition between indican and αMDG. (**A**) Steady-state I–V relations of the total current induced by αMDG and indican. The experiment was performed on an oocyte expressing hSGLT1. *Filled circles* represent the current induced by 0.25 mM αMDG alone. *Filled triangles* represent the current induced by 0.25 mM αMDG and indican (60 and 480 μM) together. *Open symbols* denote the current induced by αMDG and D-galactose together (both at 0.25 mM). (**B**) Dose–response curve (at -50 mV) of the inhibition of the current induced by 0.25 mM αMDG by increasing [indican]$_o$. *Dashed line* was drawn with a K_i of 210 μM, obtained by simulation of equation 6. Values of the kinetic parameters used for competition experiments were within the range listed in Table 1: $k_{12} = 140,000$ M^{-2}s^{-1}, $k_{21} = 300$ s^{-1}, $k_{1a} = 600$ s^{-1}, $k_{a1} = 35$ s^{-1}, $k_{ab} = 20$ s^{-1}, $k_{ba} = 15$ s^{-1}, $k_{b6} = 300$ s^{-1}, $k_{6b} = 300$ s^{-1}, $k_{25} = 0.01$ s^{-1}, $k_{52} = 3.5 \times 10^{-4}$ s^{-1}, $k_{56} = 5$ s^{-1}, $k_{65} = 2,250$ M^{-2}s^{-1}, $k_{23} = 45,000$ M^{-1}s^{-1}, $k_{32} = 20$ s^{-1}, $k_{45} = 800$ s^{-1}, $k_{54} = 81,667$ M^{-1}s^{-1}, $k_{34} = 50$ s^{-1}, $k_{43} = 50$ s^{-1}, $k_{27} = 250,000$ M^{-1}s^{-1}, $k_{72} = 12$ s^{-1}, $k_{85} = 800$ s^{-1}, $k_{58} = 756,173$ M^{-1}s^{-1}, $k_{78} = 0.5$ s^{-1}, $k_{87} = 0.5$ s^{-1}. Predicted $K_{0.5}$ for indican cotransport alone was 85 μM. In this oocyte, the currents induced at -50 mV by saturating [indican]$_o$ (600 μM) and [αMDG]$_o$ (5 mM) alone were -113 and $-1,140$ nA, respectively

210 μM. In comparison, when galactose (0.25 mM) was added to external NaCl buffer containing αMDG, the total sugar-induced current increased as expected

Fig. 4 Current records in response to a 200-ms voltage pulse protocol from an oocyte expressing hSGLT1. (**A**) In NaCl buffer. (**B**) In the presence of 100 μM indican. (**C**) In the presence of 1 mM indican. *Red traces* of (**A–C**) represent total current and *black traces* are records with the oocyte membrane capacitance subtracted. (**D–F**) Simulation of pre-steady-state currents. *Red traces* of (**D–F**) are the pre-steady-state current records for hSGLT1 at +50 and −150 mV obtained from the total current (in (**A–C**)) by subtraction of the oocyte membrane capacitance and steady-state current. Simulations (*dashed black lines*) were performed using kinetic parameters from Table 1

Pre-Steady-State Kinetics

Effect of Indican on Charge Movement

In the absence of sugar, when membrane voltage was held at −50 mV (V_h) and stepped to various test values (V_t), the magnitudes of the pre-steady-state currents were similar in the OFF voltage pulse (when V_t returned to V_h) for depolarizing and hyperpolarizing test voltages (Figs. 2A and 4A). Indican altered this profile (Figs. 2B and 4B), and at saturating concentration (1 mM), the pre-steady-state currents were observed only with depolarizing test voltages (Fig. 4C).

The $Q-V$ relations for total charge (consisting of medium and slow components) were obtained from the pre-steady-state currents (see "Materials and Methods") and fitted to the Boltzmann relation (equation 3) to obtain the maximal charge (Q_{max}), midpoint voltage ($V_{0.5}^Q$) and apparent valence of the voltage sensor ($z\delta^Q$). As previously

(Fig. 3A, open triangles). D-Galactose is transported by hSGSLT1 with a similar turnover rate and $K_{0.5}$ as αMDG (Díez-Sampedro et al. 2000).

reported, for wild-type hSGLT1 $V_{0.5}^Q$ was between −33 and −70 mV, $z\delta^Q$ was 1.0 and Q_{max} (typically ≈20 nC) depended on the level of expression of hSGLT1 on the oocyte plasma membrane (Loo et al. 1993, 2005, 2006; Quick et al. 2001). Indican shifted $V_{0.5}^Q$ to more positive values. In three experiments, when [indican]$_o$ increased from 0 to 600 μM, $V_{0.5}^Q$ shifted from −40 to + 40 mV. The dose–response relation, i.e., shift of $V_{0.5}^Q$ with [indican]$_o$, was hyperbolic with a $K_{0.5}$ ≈80 μM. Q_{max}, measured in sugar-free NaCl buffer, was reduced by 11 ± 2% in saturating indican (not shown). There was no change in $z\delta^Q$ in the presence of indican.

In contrast, for αMDG, the pre-steady-state current was abolished (>95%) by saturating concentrations of the sugar (5 mM, Fig. 2C), with a $K_{0.5}$ of 0.21 mM (present study; Loo et al. 2006). αMDG shifted the $V_{0.5}^Q$ to more positive values with a $K_{0.5}$ of 0.16 mM (Loo et al. 2006).

Effect of Indican on τ

The current records of Fig. 4A–C show that increasing concentrations of indican progressively slowed the decay of the transient current to steady state. For example,
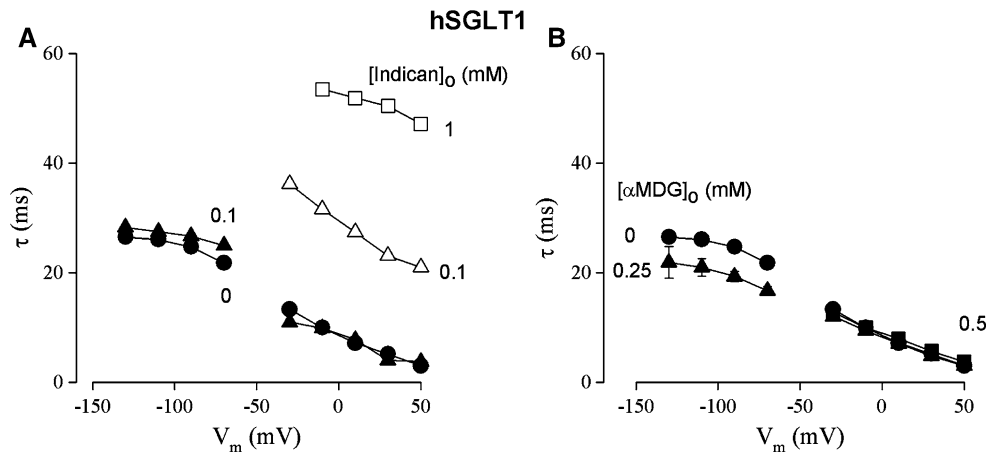
Fig. 5 Effect of indican and αMDG on relaxation time constants. (**A**) Dependence of τ–V relations for the ON response on [indican]$_o$. *Filled circles* and *triangles* (at 0 and 0.1 mM indican, respectively) represent the medium component (τ_{med}). *Open triangles* and *squares* represent the slow component (τ_{slow}) at depolarizing voltages introduced by the presence of 0.1 and 1 mM indican. At 1 mM indican, there was no detectable medium charge and no charge movement at hyperpolarizing voltages (see Fig. 4C, F). (**B**) Effect of [αMDG]$_o$ on τ–V relations. *Filled circles*, *triangles* and *squares* represent τ_{med} at 0, 0.25 and 0.5 mM [αMDG]$_o$, respectively. Charge movement for hyperpolarizing voltage pulses at 0.5 mM αMDG was too small for reliable estimates of the time constant

at $+ 50$ mV, after the initial membrane bilayer capacitance transient ($\tau \sim 0.8$ ms), to a first approximation, SGLT1 capacitive currents relaxed with a time constant (τ_{ON}) of 3 ms in the absence of indican and increased to 50 ms in 1 mM [indican]$_o$. Figure 4D–F shows the model predictions for pre-steady-state currents (dashed curves) superimposed on the compensated pre-steady-state currents (from Fig. 4A–C at test voltages of $+ 50$ and -150 mV).

A more detailed examination of the kinetics revealed that indican produced no changes in the time constant of the medium component (τ_{med}, filled symbols, Fig. 5A) but introduced a slow component with a time constant (τ_{slow}) that increased from 20 ms at 0.1 mM indican to 50 ms (at $+ 50$ mV) at 1 mM indican (open symbols, Fig. 5A). With increasing [indican]$_o$, the slow charge increased at the expense of the medium charge, and at saturating indican, only the slow charge was present.

αMDG had little effect on τ_{ON} in the depolarizing direction (Fig. 5B). For example, at $+ 50$ mV, $\tau_{ON} \approx 3.5$ ms while [αMDG]$_o$ increased from 0 to 0.5 mM. In contrast, αMDG decreased τ_{ON} at hyperpolarizing potentials, e.g., at -130 mV τ_{ON} decreased from 27 to 22 ms between 0 and 0.25 mM αMDG (Fig. 5B).

Charge Movement in the Presence of αMDG and Indican

Figure 6B shows the pre-steady-state currents in the presence of 0.25 mM αMDG. Compared to control in NaCl buffer alone (Fig. 6A), maximal charge (Q_{max}, medium component) was reduced to 37% (from 17.2 ± 0.3 to

6.4 ± 0.3 nC, Fig. 6E closed square and open circle) and $V_{0.5}^Q$ shifted from -43 ± 1 to -28 ± 3 mV (Fig. 6D, closed square and open circle). Addition of indican to the external solution with αMDG rescued Q_{max} (Fig. 6B vs. C). Maximal charge measured in 0.25 mM αMDG increased from 6.4 ± 0.4 to 15 ± 2 nC after addition of 480 μM indican and is extrapolated to be $>80\%$ of the Q_{max} in NaCl buffer alone at saturating indican (Fig. 6E, open circle and closed square). Indican also shifted $V_{0.5}^Q$ to more positive values (Fig. 6D, see also Fig. 4). There was an increase in time constant (τ_{ON} at $+ 50$ mV) with [indican]$_o$, increasing from 3.6 ± 0.2 ms in αMDG alone to 22 ± 2 ms in the presence of 480 μM indican (Fig. 6F). For the three effects of indican—shift of $V_{0.5}^Q$, increase in Q_{max} and increases in τ_{ON}—experiments and models give $K_{0.5}$ values of ~ 210 μM (Fig. 6D–F).

Fluorescence Experiments on G507C

The hSGLT1 mutant G507C was used to study protein conformations during Na$^+$/indican cotransport. This mutant exhibited similar αMDG kinetics as wild-type hSGLT1 (Loo et al. 2006), and similar $K_{0.5}^{indican}$ and $K_{max}^{indican}$ values were obtained for TMR6M-labeled and nonlabeled G507C: 75 ± 6 μM ($n = 5$) and $11 \pm 7\%$ ($n = 3$) of $I_{max}^{\alpha MDG}$. Indican had the same effect on pre-steady-state kinetics of mutant G507C as hSGLT1. For example, on the same G507C-expressing oocyte, increasing [indican]$_o$ shifted $V_{0.5}^Q$ with a $K_{0.5}$ of

Fig. 6 Pre-steady-state currents in the presence of αMDG and indican. Total current records (200 ms pulse duration) from an oocyte expressing hSGLT1. (**A**) In NaCl buffer alone. (**B**) In the presence of 0.25 mM αMDG. (**C**) In the presence of 0.25 mM αMDG and 480 μM indican together. (**D**) Dependence of $V_{0.5}^Q$ on [indican]$_o$. (**E**) Dependence of Q_{max} on [indican]$_o$. (**F**) Effect of indican on τ_{ON} (at V_t +50 mV). (**D–F**) *Filled squares* represent data obtained in sugar-free NaCl buffer, *open circles* represent data obtained in αMDG (0.25 mM) alone and *filled circles* represent data obtained in 0.25 mM αMDG and indican together. *Curves* were drawn with the $K_{0.5}$ (210 μM) obtained by simulation. Kinetic parameters used for the simulation are the same as in Fig. 3
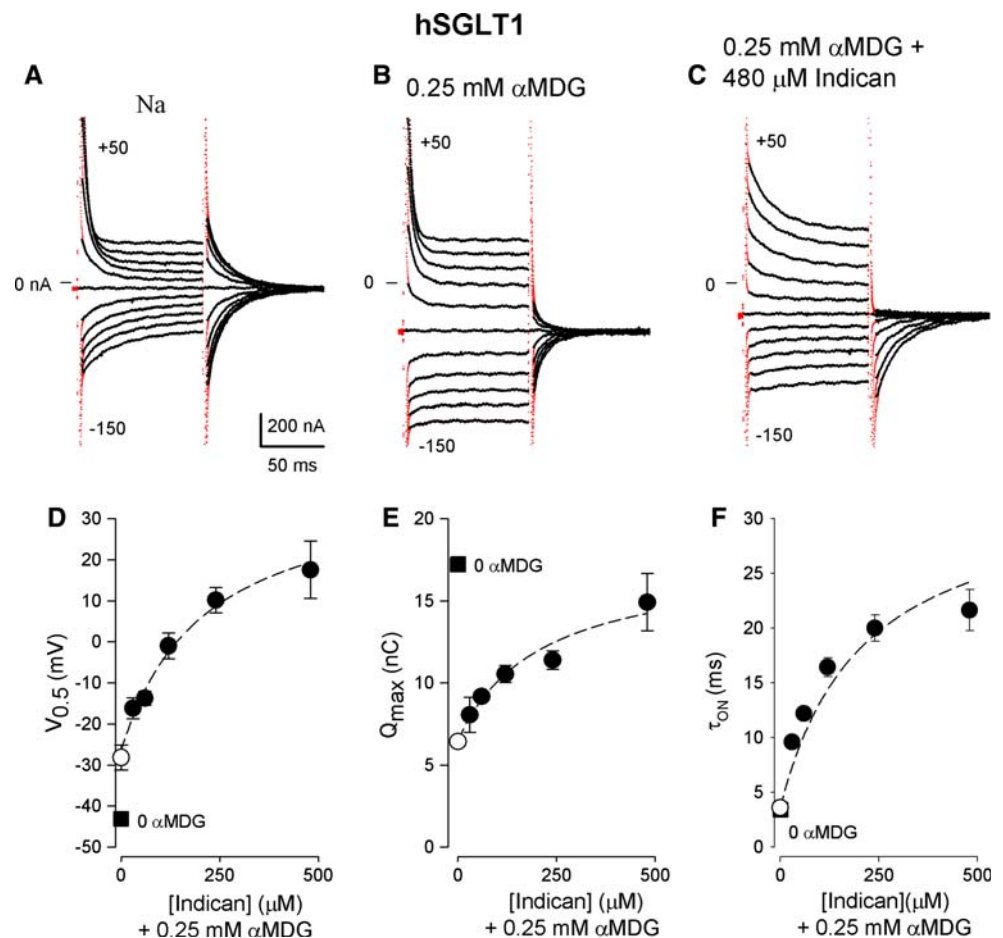
80 ± 8 μM and reduced Q_{max} by ≈10%. The time constant τ_{ON} (at + 50 mV) also increased from 4 ± 1 to 32 ± 2 ms with [indican]$_o$, with $K_{0.5}$ values of 80 ± 48 μM, respectively (data not shown).

The time course of change of rhodamine fluorescence intensity (ΔF) in NaCl buffer from an oocyte expressing hSGLT1 mutant G507C labeled with TMR6M in response to 300-ms step jumps in membrane voltage is shown in Fig. 7A. ΔF increased with depolarizing and decreased with hyperpolarizing voltages. Fluorescence intensity returned to baseline when test voltage was returned to V_h. ΔF contained medium and slow components (Loo et al. 2006). Medium time constant (τ_{med}) was sensitive to voltage: τ_{med} decreased from 15 ms at V_m −150 mV to 7 ms at + 50 mV. τ_{slow} was independent of voltage (≈ 150 ms; see also Loo et al. 2006).

The fluorescence vs. voltage ($\Delta F–V$) curves were sigmoid and fitted to Boltzmann relations to obtain the parameters ΔF_{max}, $V_{0.5}^F$ and $z\delta^F$ (see "Materials and Methods") (Loo et al. 2006). In the experiment of Fig. 7, $V_{0.5}^F$ was 7 ± 7 mV in NaCl buffer and shifted to

44 ± 13 mV in the presence of indican (600 μM). Compared to control experiments in NaCl buffer alone (Fig. 7A), in saturating [indican]$_o$ (600 μM) the extrapolated maximal fluorescence change, ΔF_{max}, increased (Fig. 7B). In three experiments, the extrapolated ΔF_{max} increased 167 ± 15%. αMDG (10 mM) shifted $V_{0.5}^F$ to more positive values (37 ± 22 mV), while ΔF_{max} was reduced by 25–50% (Fig. 7C; see also Figs. 5 and 6 of Loo et al. 2006).

Indican increased the time constants in the depolarizing direction (Fig. 7B). For example, at + 50 mV, τ_{med} increased from 10 ± 1 ms in NaCl buffer to 49 ± 5 ms ($n = 5$) in the presence of saturating [indican]$_o$. This increase in τ_{med} (at + 50 mV) was hyperbolic with [indican]$_o$, with a $K_{0.5}$ of 72 ± 35 μM ($n = 3$). τ_{slow} also increased (Fig. 7B), from 88 ± 3 to 192 ± 29 ms, when indican increased from 0 to 600 μM. In three experiments, τ_{slow} increased from 67 ± 12 to 229 ± 29 ms. The simulated fluorescence records (dashed curve) are superimposed on the experimental data (red traces) in Fig. 7D–F.

Table 1 Rate constants and parameters of the eight-state kinetic model for hSGLT1 (Fig. 8) for indican and αMDG

$k_{12} = 100{,}000$ $M^{-2}s^{-1}$	$k_{21} = 300$ s^{-1}	$\varepsilon_{12} = 0.3$	$\varepsilon_{21} = 0.3$
$k_{1a} = 600$ s^{-1}	$k_{a1} = 50$ s^{-1}	$\varepsilon_{1a} = 0.5$	$\varepsilon_{a1} \approx 0$
$k_{ab} = 5$ s^{-1}	$k_{ba} = 40$ s^{-1}	$\varepsilon_{ab} = 0.15$	$\varepsilon_{ba} \approx 0$
$k_{b6} = 100$ s^{-1}	$k_{6b} = 100$ s^{-1}	$\varepsilon_{b6} = 0.05$	$\varepsilon_{6b} = 0.7$
$k_{25} = 0.01$ s^{-1}	$^*k_{52} = 2.5 \times 10^{-3}$ s^{-1}		
$k_{56} = 5$ s^{-1}	$k_{65} = 2{,}250$ $M^{-2}s^{-1}$		
αMDG			
$k_{23} = 45{,}000$ $M^{-1}s^{-1}$	$k_{32} = 20$ s^{-1}	$K_D^o = 0.44$ mM	
$^*k_{54} = 444{,}444$ $M^{-1}s^{-1}$	$k_{45} = 800$ s^{-1}	$K_D^i = 1.8$ mM	
$k_{34} = 50$ s^{-1}	$k_{43} = 50$ s^{-1}		
Indican			
$k_{27} = 200{,}000$ $M^{-1}s^{-1}$	$k_{72} = 20$ s^{-1}	$K_D^o = 100$ μM	
$^*k_{58} = 282{,}187$ $M^{-1}s^{-1}$	$k_{85} = 400$ s^{-1}	$K_D^i = 1.4$ mM	
$k_{78} = 0.5$ s^{-1}	$k_{87} = 0.5$ s^{-1}		
Apparent quantum yields (TMR6M-labeled G507C)			
$qy_2 = 1$, $qy_1 = 3$, $qy_a = 3$, $qy_b = 3$, $qy_6 = 6$, $qy_7 = 0.7$, $qy_4 = 3$, $qy_5 = 1.6$,			
Range of validity			
$k_{12} = 50{,}000$–$140{,}000$ $M^{-2}s^{-1}$	$k_{21} = 200$–500 s^{-1}		
$k_{1a} = 400$–800 s^{-1}	$k_{a1} = 35$–50 s^{-1}		
$k_{ab} = 5$–20 s^{-1}	$k_{ba} = 15$–40 s^{-1}		
$k_{b6} = 100$–300 s^{-1}	$k_{6b} = 100$–300 s^{-1}		
Indican			
$k_{27} = 100{,}000$–$300{,}000$ $M^{-1}s^{-1}$	$k_{72} = 12$–35 s^{-1}		
$k_{85} = 100$–$1{,}000$ s^{-1}			

Apparent quantum yields

Fluorescence changes (ΔF) in Na$^+$ buffer alone are governed by the ratios $qy_6/qy_2 = 6$ and $qy_a/qy_2 = 3$. In the presence of saturating concentrations of αMDG, the highest occupancy state at negative voltages is C5Na$_2$, and the fluorescence experiments are determined by the ratio $qy_5/qy_2 \sim 1.0$–2.0. In saturating indican, the highest occupancy state at hyperpolarizing voltages is C7Na$_2$S2, and the observed increase in maximal fluorescence change (ΔF_{max}) compared to Na$^+$ buffer alone is determined by the ratio $qy_7/qy_2 \sim 0.5$–0.8. Because of the low probabilities of occupancy in C$_1$, C$_b$, C4Na$_2$S1, C8Na$_2$S2, the values of qy$_1$, qy$_b$ and qy$_4$ (or qy$_8$) were indeterminate.

The kinetic parameters were obtained by interactive numerical simulations of the model (Fig. 8) as described in the Appendix. k_{52}, k_{54} and k_{58} (marked by asterisks) are constrained by microscopic reversibility (Parent et al. 1992; Loo et al. 2006). Rate constants for Na$^+$ and αMDG binding and translocation are from Loo et al. (2006). K_D^o ($= k_{32}/k_{23}$) and K_D^i ($= k_{45}/k_{54}$) are the dissociation constants on the external and internal membrane surfaces. The internal paramers k_{56}, k_{65} and k_{45} (for αMDG) are from kinetics of reverse sugar transport (Eskandari et al. 2005). For indican transport, the reverse translocation rate (k_{87}) is assumed to be the same as the forward rate (k_{78}).

The range of validity of each kinetic parameter was obtained by examining the sensitivity of the simulations as the rate constant was varied. The range also includes the natural variation in kinetics from experiment to experiment (see Appendix)

Discussion

In our alternating access model of cotransport (Fig. 1), the interactions of a substrate with a transporter occur in three steps: binding on the external membrane surface, translocation of the substrate-bound protein across the membrane and release on the internal membrane surface. In theory, the interaction of a substrate analogue can differ in any of these steps, resulting in changes in affinity ($K_{0.5}$) or turnover (I_{max}). An understanding of the mechanism of a given analogue is important in the targeting of a transporter for delivery of a drug. In this study, we examined the mechanism underlying the differences in turnover using glucose and indican transport by SGLT1 as a model to gain insight into the binding and translocation steps of the Na$^+$/sugar cotransport cycle (Fig. 1, region II). We integrated the information from steady-state cotransporter currents and pre-steady-state charge movement and fluorescence and used the kinetic model for SGLT1 to show that the higher apparent affinity but lower turnover rate of indican compared to glucose are a consequence of both a higher affinity and a lower translocation rate across the membrane.

Each of these measurements provides unique information on how the substrate interacts with the transporter. Steady-state currents provide a measure of transport rate and yield estimates of apparent affinities ($K_{0.5}$) and maximal transport
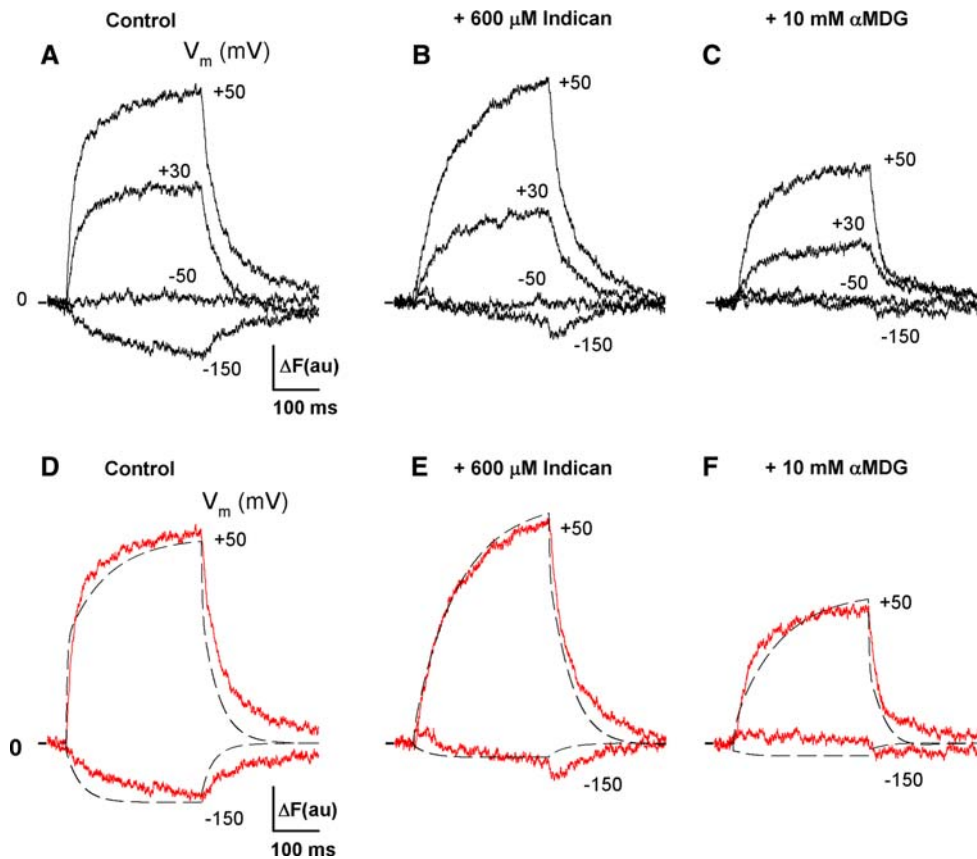
Fig. 7 Time course of the changes of fluorescence intensity (ΔF) from an oocyte expressing hSGLT1 mutant G507C labeled with TMR6M. The experiment was performed in NaCl buffer alone (**A**), with 600 µM indican (**B**) and with 10 mM αMDG added (**C**). Test pulse duration was 300 ms. V_h was –50 mV. Test voltages are indicated by the numbers next to the traces. 0 represents baseline ($\Delta F = 0$). (**D–F**) ΔF simulations on TMR6M-labeled hSGLT1 mutant G507C. *Red traces* are from (**A–C**) above (at +50 and –150 mV). *Black dashed lines* are simulated ΔF records (with steady-state fluorescence levels removed) when V_m is stepped from –50 mV to +50 and –150 mV. Simulations were performed using the set of kinetic parameters for αMDG obtained for the TMR6M-labeled

mutant (Table 1 but with αMDG binding rate $k_{23} = 8,000$ M^{-1}s^{-1} to account for the lower apparent affinity of G507C for αMDG) (Loo et al. 2006). Rate constants for indican transport by TMR6M-labeled G507C were the same as for hSGLT1 since the kinetics of indican transport were similar between the two proteins. Relative quantum yield values were $qy_1 = 3$, $qy_2 = 1$, $qy_a = 3$, $qy_b = 3$, $qy_3 = 0.7$, $qy_4 = 3$, $qy_5 = 3$ and $qy_6 = 5$–6. In practice, ΔF in the presence of αMDG was determined by relative quantum yields $qy_5/qy_2 \approx 3$, and $qy_6/qy_2 \approx 6$ (Loo et al. 2006); in indican, an additional constraint was $qy_6/qy_7 \approx 8$. See Table 1 for the range of validity of the parameters

rate (I_{max}). Charge movements in the Na$^+$/glucose cotransport cycle are associated with external Na$^+$ binding and translocation of the empty transporter (Fig. 1, region I) and provide a monitor of the conformational state distribution of the protein. A decrease in charge movement in the presence of a substrate (e.g., αMDG) is the result of depopulation or reduction of occupancy in the "charge-associated" conformations (Fig. 1, region I). Thus, the abolition of charge movements by αMDG and the minor 10% reduction by indican indicate that the distribution of conformational states of hSGLT1 differs in αMDG and indican; i.e., there is a difference in the rate-limiting conformation changes for indican and αMDG transport.

The turnover rate for a substrate is estimated from the ratio of the maximal rate of transport (I_{max}) and maximal

charge (Q_{max}) (Loo et al. 1993). The turnover rate for αMDG transport by hSGLT1 has been estimated to be 28 s^{-1} (Loo et al. 2005). Since indican is transported at 10% of the maximal rate of αMDG, the turnover rate for indican is 2.8 s^{-1}.

Fluorescence is also an indicator of changes in conformational state distribution. The changes in rhodamine fluorescence (with substrates and membrane voltage) could be due to a Stokes shift or a quench of fluorescence (Bezanilla 2000). In the SGLT1 homologue vSGLT from *Vibrio parahaemolyticus* (Veenstra et al. 2004) and hSGLT1 mutant Q457C (unpublished data), the sugar-induced quenches of fluorescence of covalently linked extrinsic fluorophores are not accompanied by shifts in absorption or emission spectra.
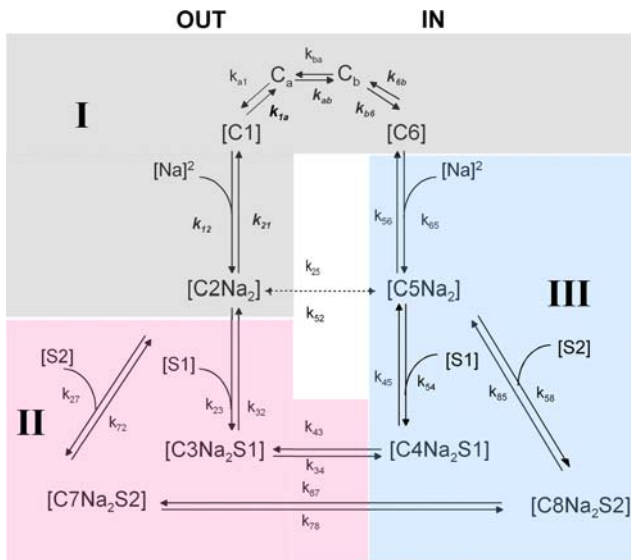
Fig. 8 Ten-state kinetic model for SGLT1 in the presence of αMDG (S1) and indican (S2). Compared to the eight-state model (Fig. 1), there are two additional states, indican-bound C_7 ([C7Na$_2$S2]) and C_8 ([C8Na$_2$S2]). Colored regions (I–III) are as described in Fig. 1. Rate constant (k_{ij}) represents the transition between states ($C_i \rightarrow C_j$). Those italized and in bold (k_{12}, k_{21}, k_{1a}, k_{ab}, k_{b6}, k_{6b}) are voltage-dependent. The effects of voltage were described by Eyring rate theory: $k_{ij} = k_{ij}^o \exp(-\varepsilon_{ij}FV/RT)$, where k_{ij}^o is a voltage-independent rate, ε_{ij} is the equivalent charge movement and F, R and T have their usual physicochemical meanings (see Loo et al. 2005, 2006). Rate constants obey microscopic reversibility conditions: $k_{52}^o k_{21}^o k_{1a}^o k_{ab}^o k_{b6}^o k_{65}^o = k_{12}^o k_{25}^o k_{56}^o k_{6b}^o k_{ba}^o k_{a1}^o$, $k_{54}^o k_{43}^o k_{32}^o k_{25}^o = k_{45}^o k_{52}^o k_{23}^o k_{34}^o$ (for αMDG transport) and $k_{58}^o k_{87}^o k_{72}^o k_{25}^o = k_{85}^o k_{52}^o k_{27}^o k_{78}^o$ (for indican transport). The differential equation of the model is equation 6. The parameters estimated for indican and αMDG are listed in Table 1. In this study, intracelluar [αMDG] and [indican] were 0 and intracelluar [Na$^+$] was 5 mM

The fluorescence associated with SGLT1 (on the population level) is the sum of the fluorescence from the transporter distributed in different conformations (depending on ligand concentration and membrane voltage). The binding of a ligand (Na$^+$ or sugar) and/or a change in membrane voltage alters the distribution of conformations, resulting in a change of fluorescence (see equation 5; Loo et al. 2006). Fluorescence measurements have the advantage over charge movements in that they can also monitor conformational changes that are electrically silent. While charge measurements monitor global conformational changes, the fluorescence changes arise from local changes of the environment of the fluorophore responding to remote electrical events and/or ligand binding.

The fluorescence measurements provide us with additional insight into sugar interactions with SGLT1: (1) in saturating [αMDG]$_o$, the charge movement is abolished whereas the fluorescence signal is not (Fig. 7F), indicating that the conformational change monitored by fluorescence (C5Na$_2$ to C6) is electrically silent (Loo et al. 2006); (2) there is an increase in fluorescence with increasing [indican]$_o$, confirming the evidence of a sugar- (indican) bound conformation (C7Na$_2$S, Fig. 8); (3) the increase of fluorescence indicates that there is a change of the local environment of the fluorophore between the Na$^+$-bound (C2Na$_2$) and the fully loaded Na$^+$ and indican-bound (C7Na$_2$S) conformations, thereby providing direct evidence for a conformational change of hSGLT1 after sugar binding, and this sugar binding step has not been previously examined by electrical measurements because it is voltage-independent (Parent et al. 1992; Loo et al. 2006); and (4) the contrast between the increase of fluorescence in saturating [indican]$_o$ and the decrease of fluorescence in saturating [αMDG]$_o$ indicates that the rate-limiting conformation is different between αMDG and indican.

In summary, the charge and fluorescence measurements indicate a difference in the rate-limiting step (and conformation) for indican and αMDG transport. For indican it is sugar translocation across the membrane, whereas for αMDG it occurs on the internal membrane surface. The recovery of the charge lost in the presence of αMDG by increasing concentrations of indican (Fig. 6E) indicates that competition between indican and αMDG is due to a higher affinity of SGLT1 for indican and a lower turnover rate for indican, thereby "trapping" the transporters in the indican-bound conformation (C7Na$_2$S). To examine this interpretation, computer simulations were performed on the kinetic model for SGLT1 (Loo et al. 2006).

Kinetic Model

The kinetic model for SGLT1 is based on the alternating access mechanism with a Na$^+$/substrate transport stoichiometry of 2 (Fig. 8). The transporter is assumed to have eight kinetic states, consisting of the empty (C1 and C6), Na$^+$-bound (C2Na$_2$ and C5Na$_2$) and Na$^+$- and sugar-bound (C3Na$_2$S1 & C4Na$_2$S1 for glucose and C7Na$_2$S2 & C8Na$_2$S2 for indican) states at the external and internal membrane surfaces, as well as intermediate states (C$_a$ and C$_b$) between C1 and C6. The empty or ligand-free protein is negatively charged (valence −2). The voltage-sensitive steps are the binding of external Na$^+$ (C1 to C2Na$_2$) and the translocation of the empty carrier between the external and internal sides of the membrane (C1 to C6). SGLT1 pre-steady-state currents are associated with the voltage-sensitive partial reactions (see Appendix for details on the formulation of the model and estimation of the kinetic parameters). Fluorescence experiments were simulated by attributing empirical (or apparent) quantum yield values for the fluorophore in each conformation of the transporter and assuming that changes of fluorescence intensity (ΔF) are due to changes in occupancy probabilities as membrane

voltage and substrate concentrations are altered (see equation 5; Loo et al. 2006).

Model Simulations

Simulations were performed on the eight-state kinetic model by estimating the rate constants for αMDG and indican transport alone, and this was extended to a 10-state model in the presence of both sugars (see Fig. 8). As described below, we were able to simulate the experimental data on (1) steady-state kinetics—the *I–V* relations of the sugar- (indican, αMDG) coupled currents (Fig. 2D) and the $K_{0.5}$ and I_{max} values for indican and αMDG; (2) competition between indican and αMDG (Figs. 3B, 6D–F, 7D–F); and (3) differences in pre-steady-state kinetics of charge and fluorescence in the presence of indican and αMDG (Fig. 4D–F).

Indican and αMDG Alone

The kinetic parameters extracted from the simulations for indican (this study) along with those previously obtained for glucose (αMDG) are summarized in Table 1. Indican and αMDG differed in their binding affinities and translocation rates. The external binding constants (K_D) for indican and αMDG are 40 μM and 0.44 mM, respectively. The rate of translocation of αMDG across the cell membrane (k_{34} 50 s^{-1}) was 100-fold greater than that of indican (k_{78} 0.5 s^{-1}). Model predictions fit the experimental data on the steady-state *I–V* relations and the $K_{0.5}$ and I_{max} values for indican and αMDG (Fig. 2D, E).

The rate-limiting step of the transport cycle under maximal transport conditions—large hyperpolarizing voltages and saturating external sugar and sodium concentrations—is the sugar-translocation step ($k_{78} = 0.5$ s^{-1}) for indican, whereas it is the release of Na$^+$ from SGLT1 in the internal membrane surface ($k_{56} = 5$ s^{-1}) for αMDG (Table 1). This finding is also supported by the observed low apparent affinities (by two orders of magnitude) for sugars and glycosides on the internal membrane surface compared to the external (Eskandari et al. 2005).

The effects of sugars (indican and αMDG) on occupancy probabilities (P_o) of the eight-state model are shown in Fig. 9. In the absence of sugar (100 mM [Na$^+$]$_o$ alone) the protein resides in the outward-facing Na$^+$-bound conformation C2Na$_2$ at large hyperpolarizing voltages (<-150 mV) and in the inward-facing empty transporter state C6 at large depolarizing voltages ($>>+50$ mV) (Fig. 9A). In saturating [indican]$_o$ (1 mM), the highest occupancy state at -150 mV is the outward-facing Na$^+$ and indican-bound conformation C7Na$_2$S2 ($P_o = 0.8$, Fig. 9B). In contrast, the highest occupancy state in saturating [αMDG]$_o$ (10 mM) is the inward-facing Na$^+$-bound conformation C5Na$_2$

($P_o = 0.7$ at -150 mV, Fig. 9C). In all cases, at large depolarizing voltages ($>>+50$ mV) the protein is driven to the inward-facing ligand-free conformation C6. The differences in state occupancy at negative membrane potentials (e.g., -50 mV) provide the rationale for the observed charge movement in saturating indican and its disappearance in saturating αMDG. A depolarizing voltage pulse (e.g., from V_h -50 to $+50$ mV) in saturating indican would drive SGLT1 from C7Na$_2$S2 to C$_6$ (along the conformations in Fig. 1, region I), thereby generating a pre-steady-state outward current, while a hyperpolarizing pulse (from -50 to -150 mV) only causes a minor increase in C$_7$Na$_2$S2 at the expense of C5Na$_2$ and, thus, a small pre-steady-state inward current. In contrast, there are negligible pre-steady-state currents in saturating [αMDG]$_o$ as extreme voltage jumps only alter the distribution of the transporter between electroneutral steps (C5Na$_2$ and C$_6$, Fig. 9C).

There was close agreement between the simulated pre-steady-state currents and the experimental compensated pre-steady-state current, and this is shown in Fig. 4D–F for 0 μM, 100 μM and 1 mM indican. Likewise, there was good agreement between simulated ΔF records and experimental data (Fig. 7D–F). The increase in maximal fluorescence (ΔF_{max}, extrapolated) at saturating indican (Fig. 7E) is due to a lower (apparent) quantum yield of C7Na$_2$S2 compared to C2Na$_2$, whereas the decrease at saturating αMDG (Fig. 7F) is due to the lower (apparent) quantum yield of C5Na$_2$ compared to C$_6$ (Fig. 9C) (Loo et al. 2006). The fluorescence change (ΔF) when V_m is stepped from -50 mV (V_h) to $+50$ mV is associated with transition from C5Na$_2$ → C$_6$ in saturating αMDG, whereas it arises from C7Na$_2$S2 → C$_6$ (along region I of Fig. 1, see also Fig. 5B, C) in saturating indican.

Competition Between Substrates

We have shown that indican acts as an inhibitor of αMDG transport (Fig. 3). This was at first surprising as we expected that the currents for the two sugars would be additive, as for αMDG and galactose (Fig. 3A). The inhibition can be understood from the state distributions of hSGLT1 in the presence of the two competing sugars. Compared to the distribution in the absence of sugar where the transporter is in C2Na$_2$ at large hyperpolarizing voltages (Fig. 9A), the transporter is distributed between C5Na$_2$ (P_o 0.5) and C2Na$_2$ (P_o 0.3) at 0.25 mM [αMDG]$_o$ (Fig. 10A). When a saturating [indican]$_o$ (1 mM) is added in the presence of 0.25 mM [αMDG]$_o$, the transporter is predominantly in the indican-bound configuration C7Na$_2$S2 ($P_o = 0.7$, Fig. 10B). The increase in C$_7$Na$_2$S2 occurs at the expense of C$_5$Na$_2$. Thus, the inhibition is simply due to competitive inhibition between indican and αMDG for the external binding site and the very low

Fig. 9 Simulation of occupancy probabilities (P_o). (**A**) In NaCl buffer in the absence of sugar. (**B**) In saturating indican (1 mM). (**C**) In saturating αMDG (10 mM). *Vertical dashed lines* in (**A**–**C**) show the values of P_o at holding potential (–50 mV). Simulated time course of P_o for a 300-ms voltage pulse from V_h (–50 mV) to +50 mV in Na$^+$ alone (**D**), saturating indican (**E**) and saturating αMDG (**F**). Simulations were performed using the kinetic parameters of Table 1. For clarity, states with $P_o < 0.1$ were not plotted; these states were C$_1$ in (**A**) (and (**D**)); C$_1$, C2Na$_2$, C3Na$_2$S1, C4Na$_2$S1, C8Na$_2$S2 in (**B**) (and (**E**)); and C$_1$, C2Na$_2$, C3Na$_2$S1, C4Na$_2$S1, C7Na$_2$S2, C8Na$_2$S2 in **C** (and **F**)
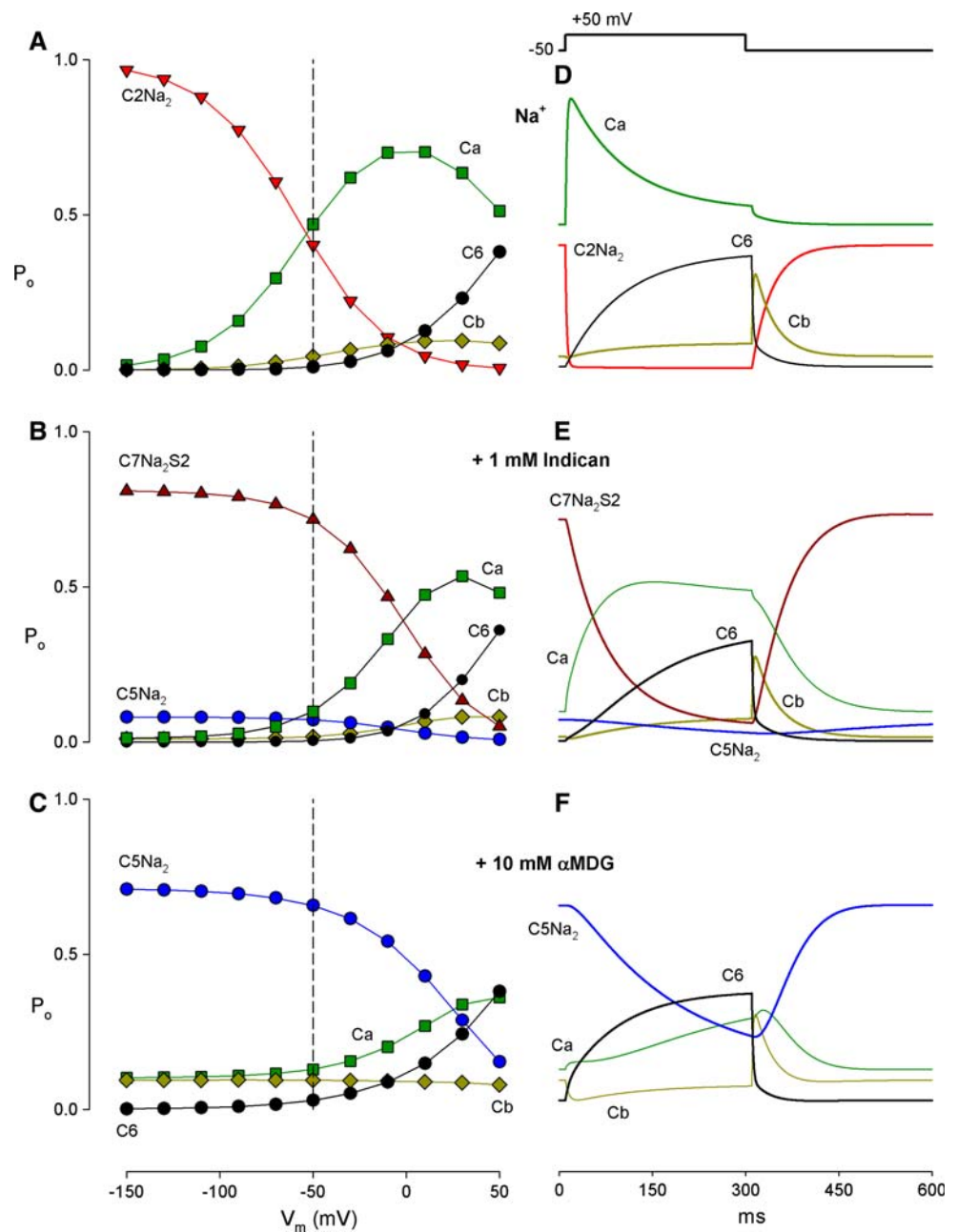
translocation rate of indican relative to αMDG, k_{78} 0.5 vs. k_{34} 50 s^{-1} (Table 1).

Simulation predicted that the $K_{0.5}$ for the inhibition of the total 0.25 mM sugar-coupled current by indican is 210 μM (dashed line, Fig. 3B), close to the experimental value of 247 ± 84 μM. These values are higher (60–100 μM) than the experiment and simulated values of $K_{0.5}$ (85 μM) in indican alone. Simulations indicate that if αMDG is present at the $K_{0.5}$ concentration, then K_i for indican inhibition of αMDG current was twice the $K_{0.5}$ for indican transport with no change in the maximum velocity, i.e., classical competitive inhibition. Irrespective of the fixed indican concentration, in theory, a sufficiently high

αMDG concentration can be obtained to outcompete indican binding. The $K_{0.5}$ for the shift of $V_{0.5}^Q$, the increase in Q_{ma}, and the increases in τ_{ON} with increasing [indican]$_o$ were similar to the $K_{0.5}$ (210 μM) for the inhibition of αMDG-currents (Fig. 5D–F).

In summary, our model simulations reproduce the key new observations of this study: (1) indican behaved as an inhibitor of αMDG transport; (2) indican had little effect on hSGLT charge movement, whereas αMDG abolished them; (3) indican increased the time constants for hSGLT1 capacitive currents, up to 20-fold, whereas αMDG had little effect; and (4) indican increased the voltage-dependent fluorescence of TMRM6-G507C-hSGLT1 (ΔF_{max}) to
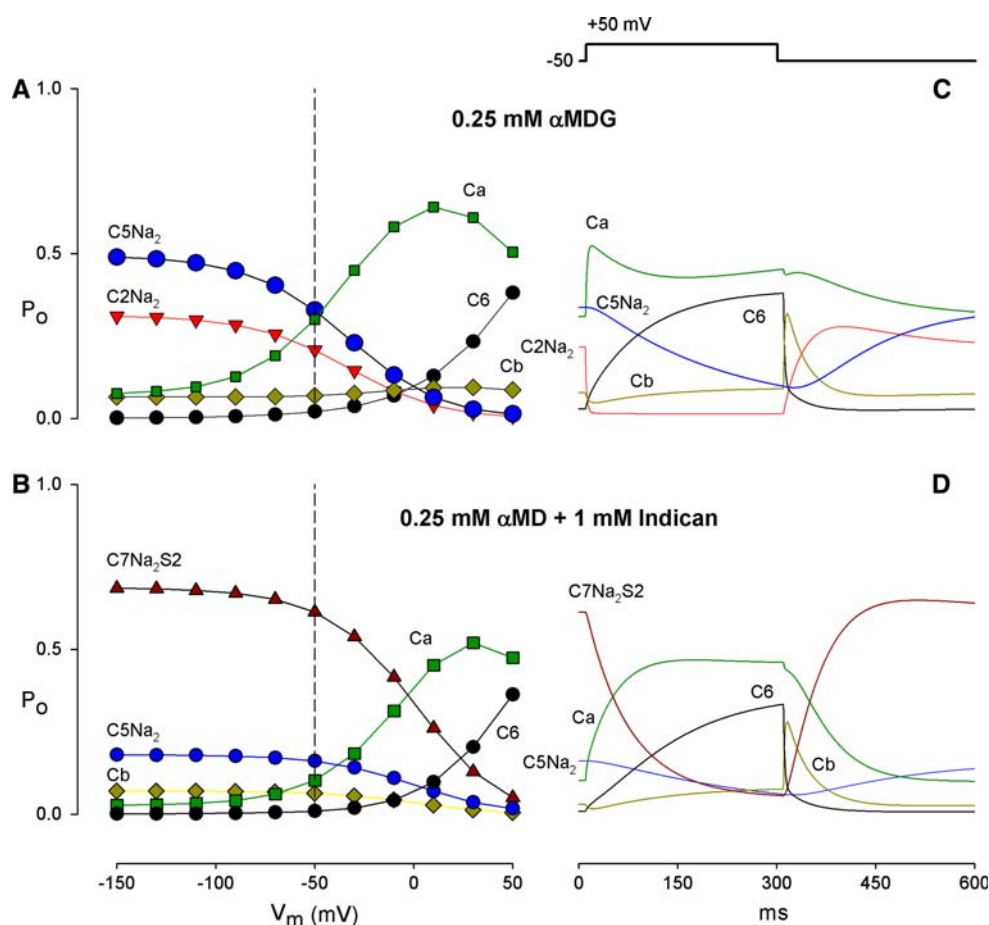
Fig. 10 Simulation of occupancy probabilities (P_o) in the presence of αMDG and indican. The 10-state model (Fig. 8) was used for simulations. C3Na$_2$S1 and C4Na$_2$S1 are αMDG-bound. C7Na$_2$S2 and C8Na$_2$S2 are indican-bound. (**A**) In the presence of αMDG (0.25 mM) alone. (**B**) In the presence of αMDG (0.25 mM) and indican (1 mM). *Vertical dashed lines* show the values of P_o at holding potential (−50 mV). (**C**) Simulated time course of P_o for a 300-ms voltage pulse from V_h (−50 mV) to +50 mV in αMDG alone. (**D**) Simulated time course

of P_o in αMDG and saturating indican. The simulated time course of P_o in 100 mM [Na$^+$]$_o$ alone is shown in Fig. 9D. Simulations were performed using the kinetic parameters of Table 1. For clarity, states with $P_o < 0.1$ were not plotted. The states were C$_1$, C3Na$_2$S1 (αMDG-bound) and C4Na$_2$S1 (αMDG-bound) in (**A**) and (**C**); C$_1$, C2Na$_2$, C3Na$_2$S1 (αMDG-bound), C4Na$_2$S1 (αMDG-bound) and C8Na$_2$S2 (indican-bound) in (**B**) and (**D**)

150%, whereas αMDG reduced this signal to 30%. The overall goodness of fit between model simulations and experimental data provides further confirmation of the eight-state kinetic model for SGLT1 (Loo et al. 2006).
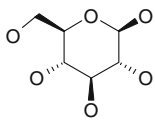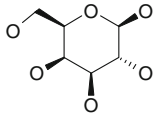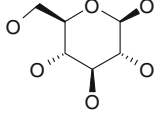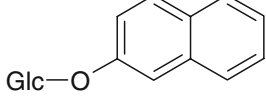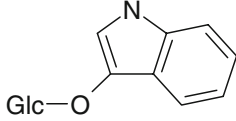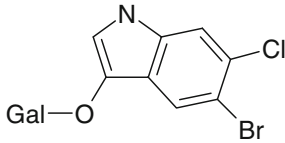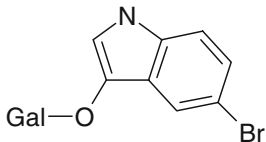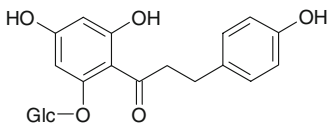
Distinction Between Substrates and Competitive Inhibitors

A single cotransporter may transport substrates with wide differences in apparent affinities and maximal transport rates. Thus, in the transport cycle, there is a "specificity" for substrate binding that may be different from the specificity for translocation. The apparent affinity largely depends on the rate constants for substrate binding (k_{23}, k_{32} or k_{27}, k_{72}). Maximum transport rate largely depends on the rate-limiting step: k_{78} (for indican) and k_{56} (for αMDG). Indican binding is fivefold stronger than αMDG binding, while the translocation rate is 100-fold lower (Table 1).

This leads to indican acting as a competitive inhibitor of αMDG transport.

There is no simple relationship between the structure of the compounds and their transport rate (Table 2). Glucosides such as 2-naphthyl-β-D-glucopyranoside bind with the same apparent affinity ($1/K_{0.5}$) as αMDG but have low turnover numbers (8% of αMDG). Likewise, simple halogenation of indican, e.g., 5-bromo- and 5-bromo-6-chloro-3-indolyl-β-galactose, produced inhibitors of αMDG transport with K_i values of 40–200 μM. This means that the rate of translocation (k_{34}) of these blockers approached 0. As with indican, the blockers did not inhibit charge movement but, instead, increased the time constant at +50 mV and shifted $V_{0.5}^Q$ to more positive values (Hirayama et al. 2001). With very high-affinity blockers, e.g., phlorizin (K_i 200 nM), there was complete inhibition of charge movement, i.e., during a 100-ms

Table 2 Kinetics of glycoside interactions with hSGLT1

Compound	Structure	Transport rate (%)	$K_{0.5}$ (mM)	K_i (mM)
D-Glucose		100	0.5[2]	–
D-galactose		100	0.5[2]	–
α-Methyl-D-glucose		100	0.5[1,2]	–
2-Naphthyl-β-D-glucose		8	0.5[3]	–
Indican (indoxyl-β-D-glucose)		12	0.07[3]	–
5-Br-6Cl-3-indoxyl-galactose		0	–	0.038[3]
5-Br-3-indoxyl-galactose		0	–	0.060[3]
Phlorizin		0	–	0.0002[1,4]

Half-maximal concentration ($K_{0.5}$) or inhibitory (K_i) constants, structures and transport rates of various glycosides. References: [1]Hirayama et al. 1996; [2]Díez-Sampedro et al. 2001; [3]Díez-Sampedro et al. 2000; [4]Loo et al. 2006

depolarizing pulse to + 50 mV there was no dissociation of the blocker from the transporter (Loo et al. 2006). We surmise that the aglycone binds to a specific binding site within 8 Å of the external glucose binding site on hSGLT1 (Hirayama et al. 2001) and that this high binding energy precludes translocation. In the case of phlorizin, the high binding energy locks the transporter in C3Na$_2$S1, disabling transport and charge movement. With lower-affinity phlorizin binding, e.g., to the TMR6M-labeled hSGLT1 mutant Q457C with a K_i of 100 μM, charge transfer was recovered by holding the membrane potential at + 50 mV for 5 s (Loo, Hirayama, Meinild and Wright, unpublished data).

Pharmacological Relevance

In the present and previous studies (Díez-Sampedro et al. 2000, 2001), we have highlighted that SGLT1 can transport a wide variety of sugars with apparent affinities ($K_{0.5}$) ranging from 50 μM to 100 mM and with similar or very different maximal rates of transport (15–100% of that for glucose). The transport of substrate analogues with different turnover rates is a common observation among transporters. There are strong parallels between the present findings on αMDG and indican transport by hSGLT1 and the transport of physiological substrates uridine and adenosine by rat nucleoside transporter CNT1 (Yao et al. 1996).

Uridine and adenosine are transported with similar apparent affinities (26 μM), but maximal rate of adenosine transport is only 0.33% of that for uridine. Return of the empty transporter from the inward-facing to the outward-facing conformation is thought to be rate-limiting for uridine transport, whereas translocation across the membrane is thought to be the rate-limiting step for adenosine transport.

The nucleoside (hCNT1, hCNT3, NUpC) and dipeptide (hPEPT1, hPEPT2) cotransporters (Veyhl et al. 1998; Loewen et al. 2004; Knutter et al. 2007; Sala-Rabanal et al. 2006; Larrayoz et al. 2004; Smith et al. 2004; King et al. 2006) are of particular pharmacological interest since their broad substrate specificity makes them suitable targets for drug delivery. Their substrate analogues include anticancer drugs and antibiotics. For example, gemcitabine, a pyrimidine analogue of deoxycytidine, is an anticancer drug transported by human CNT1 with a twofold higher affinity ($K_{0.5}$ 24 vs. 45 μM) but a four- to fivefold lower maximal rate than uridine (Mackey et al. 1999). Likewise, the $β$-lactam antibiotic cefadroxil is transported by human PEPT2 with an approximately fourfold higher affinity ($K_{0.5}$ 0.27 vs. 1.2 mM) but an approximately twofold lower maximal rate than glycylsarcosine (Sala-Rabanal et al. 2008).

The differences in affinities and turnover numbers could result in significant inhibition of transport of the natural substrate, making interactions between different substrates for a transporter of considerable interest. For example, indican is a natural plant glucoside and is just one example of the glucosides in "dietary supplements" that are widely touted as natural folk medicines. A common question in nutrition circles concerns the adsorption of such glucosides in the gut. Many of these glucosides, like indican, may interact with or bind to SGLT1, and the interactions such as we describe here may have beneficial or adverse effects on the normal adsorption of glucose, e.g., blunt glucose adsorption after a meal; be useful in the treatment of diabetes; or cause diarrhea. We further cite two examples of the interaction of "drug" substrates with transporters; first is the transport of glufosfamide, a glycoside in clinical trials for pancreatic cancer (Briasoulis et al. 2000). Glufosfamide is a high-affinity, low-turnover substrate for SGLT1 and SGLT3 (Veyhl et al. 1998; unpublished results) and may block glucose uptake into cells. Second is the oral delivery of drugs where the drug may reduce the absorption of natural dipeptides by direct competition and a reduction in the maximum velocity of hPEPT1 (Sala-Rabanal et al. 2006).

Summary

We have examined the kinetics of indican transport using biophysical methods and mathematical modeling. The lower turnover rate of indican compared to glucose is due to differences in the rate-limiting step: for indican it is sugar translocation, whereas for glucose it is dissociation of Na$^+$ from the internal binding sites. Indican may act as an inhibitor of glucose transport due to its higher affinity and lower transport rate. The kinetics of indican and glucose transport, alone or together, can be accounted for by the model; and this shows the utility of kinetic models in understanding how substrates influence the transport mechanism. The interactions between low- and high-turnover substrates have implications in the use of cotransporters as drug delivery systems. We also demonstrate that fluorescence measurements combined with steady-state and presteady-state kinetic analysis provide powerful tools for studying the partial reactions of the transport cycle.

Appendix

This focuses on the formulation and simulation of the kinetic model for SGLT1 in the presence of indican and αMDG, alone and together.

Kinetic Model

The model is based on extensive experimental data (Parent et al. 1992; Loo et al. 1993, 1998, 2005, 2006; Hirayama et al. 1997, 2007; Meinild et al. 2002; Eskandari et al. 2005; Mackenzie et al. 1998, Zampighi et al. 1995). The transporter has eight kinetic states: ligand-free (empty), Na$^+$-bound, Na$^+$- and sugar-bound, and intermediates (C_a, C_b) between the inward- and outward-facing empty conformations (Fig. 8). The empty protein has a valence of -2, and the voltage-sensitive steps are the binding of external Na$^+$ (C1 to C2Na$_2$) and translocation of the empty carrier between the external and internal sides of the membrane (C1–C6).

Transitions between states C_i and C_j are represented by first-order (or pseudo-first-order in case of Na$^+$ and sugar binding) rate constants k_{ij}: $C_i \rightarrow C_j$. Eyring rate theory is used to describe the dependence of rate constants on membrane potential. $k_{ij} = k_{ij}^o \exp(-\varepsilon_{ij}F/RT)$, where k_{ij}^o is a voltage-independent rate, ε_{ij} is the equivalent charge movement (up to the transition state between $C_i \rightarrow C_j$) and F, R and T have their usual physicochemical meanings (Parent et al. 1992). Na$^+$ and sugar binding on external and internal membrane surfaces is represented by pseudo-rate constants $k_{12} = k_{12}^o$

$[Na]_o^2 \exp(-\varepsilon_{12}FV/RT), k_{23} = k_{23}^o[\alpha MDG]_o, k_{27} = k_{27}^o[\text{indi-can}]^o, k_{65} = k_{65}^o[Na]_i^2$ and $k_{54} = k_{54}^o[\alpha MDG]_i, k_{85} = k_{85}^o$ [indican]$_i$. Na$^+$ ions bind to two identical binding sites in one step before glucose (C1 + 2Na$^+$ ⇌ C2Na$_2$), and this is considered to be valid at high [Na$^+$]$_o$ with high cooperativity between Na$^+$ binding sites (Falk et al. 1998).

Pre-steady-state currents (hSGLT1 capacitive currents) are associated with the reorientation of the empty carrier between outward- and inward-facing conformations (C1 ⇌ C$_a$ ⇌ C$_b$ ⇌ C6) and external Na$^+$ binding/dissociation (C1 ⇌ C2Na$_2$). There are four predicted components of pre-steady-state currents (region I, Figs. 1 and 8): C$_2$Na$_2$ ⇌ C$_1$, C$_1$ ⇌ C$_a$, C$_a$ ⇌ C$_b$, and C$_b$ ⇌ C$_6$. The current (I_{ij}) associated transition C$_i$ ⇌ C$_j$ is given by $I_{ij} = e(\varepsilon_{ij} + \varepsilon_{ji})(k_{ij}C_i - k_{ji}C_j)$, where e is elementary charge (Loo et al. 2005; Parent et al. 1992).

Total current (I) associated with SGLT1 is

$$I = N_T (I_{12} + I_{1a} + I_{ab} + I_{b6})$$
$$= N_T e[(\varepsilon_{12} + \varepsilon_{21})(k_{12}C_1 - k_{21}C_2Na_2)$$
$$+ (\varepsilon_{1a} + \varepsilon_{a1})(k_{1a}C_1 - k_{a1}C_a) + (\varepsilon_{ab} + \varepsilon_{ba})(k_{ab}C_a - k_{ba}C_b)$$
$$+ (\varepsilon_{b6} + \varepsilon_{6b})(k_{b6}C_b - k_{6b}C_6)] \tag{4}$$

where N_T is the total number of transporters in the oocyte plasma membrane.

Changes of fluorescence intensity (ΔF) associated with SGLT1 with step jumps in membrane voltage are assumed to be due to changes in occupancy probabilities:

$$\Delta F \approx qy_1\Delta C_1 + qy_2\Delta C_2 + qy_a\Delta C_a + qy_b\Delta C_b + qy_3\Delta C_3$$
$$+ qy_4\Delta C_4 + qy_5\Delta C_5 + qy_6\Delta C_6 \tag{5}$$

where qy_j is the apparent quantum yield of the fluorophore (TMR6M) when SGLT1 is in conformation C$_j$ (Loo et al. 2006).

Simulation of SGLT1

In the presence of two different substrates the model has 10 states (Fig. 8), with the differential equation (equation 6):

C_i is the occupancy probability in state i and $C_1 + C_2 + C_3 + C_4 + C_5 + C_6 + C_7 + C_8 + C_a + C_b = 1$. In case of a single substrate, equation 6 reduces to equation 4 of Loo et al. (2006).

Computer simulations were performed using Berkeley Madonna 8.0.1 (Loo et al. 2006). The voltage pulse protocol was simulated by determining the occupancy probabilities at holding potential ($V_h = -50$ mV). At each test voltage (V_t ranging between $+50$ and -150 mV), the time course of the occupancy probabilities was obtained by numerically integrating equation 6. Cotransporter currents and fluorescence intensity changes (ΔF) were calculated using equations 4 and 5. Steady-state kinetic parameters ($I_{max}, K_{0.5}$) were simulated by generating the I–V relations for the sugar-coupled current as functions of [Na$^+$]$_o$ and [sugar]$_o$. At each V_m, the I vs. [sugar]$_o$ and I vs. [Na$^+$]$_o$ curves were fitted to equation 1.

For pre-steady-state simulations, the predicted transient cotransporter currents for ON and OFF responses at each voltage (V) were integrated to obtain the charge (Q). $Q-V$ relations were fitted with the Boltzmann relation (equation 3) to obtain $Q_{max}, z\delta^Q$ and $V_{0.5}^Q$. Model predictions on relaxation time constants were obtained by fitting the simulated pre-steady-state currents to

$$I(t) = I_{fast} \exp(-t/\tau_{fast}) + I_{med} \exp(-t/\tau_{med})$$
$$+ I_{slow} \exp(-t/\tau_{slow}) + I_{ss} \tag{7}$$

$I_{fast}\exp(-t/\tau_{fast})$ is the fast submillisecond component and is beyond the resolution of the two-electrode voltage clamp (Loo et al. 2005).

Estimating Kinetic Parameters

In two-electrode voltage-clamp experiments, the rate constants for sugar translocation (C3Na$_2$S1 ⇌ C4Na$_2$S1) and internal ligand binding (C4Na$_2$S1 ⇌ C5Na$_2$ + S1; C5Na$_2$ ⇌ C6 + 2Na$^+$) cannot be uniquely determined. This requires the kinetics of outward currents, using, e.g., excised patches (Eskandari et al. 2005). Here, we used kinetic parameters obtained from experiments where

$$\frac{d}{dt}\begin{bmatrix} C_1 \\ C_2 \\ C_3 \\ C_4 \\ C_5 \\ C_6 \\ C_7 \\ C_8 \\ C_a \\ C_b \end{bmatrix} = \begin{bmatrix} -(k1a+k12) & k21 & 0 & 0 & 0 & 0 & 0 & ka1 & 0 \\ k12 & -(k21+k23+k25+k27) & k32 & 0 & k52 & 0 & k72 & 0 & 0 & 0 \\ 0 & k23 & -(k32+k34) & k43 & 0 & 0 & 0 & 0 & 0 \\ 0 & 0 & k34 & -(k43+k45) & k54 & 0 & 0 & 0 & 0 \\ 0 & k25 & 0 & k45 & -(k52+k54+k56+k58) & k65 & 0 & k85 & 0 & 0 \\ 0 & 0 & 0 & 0 & k56 & -(k65+k6b) & 0 & 0 & kb6 \\ 0 & k27 & 0 & 0 & 0 & 0 & -(k72+k78) & k87 & 0 & 0 \\ 0 & 0 & 0 & 0 & k58 & 0 & k78 & -(k85+k87) & 0 & 0 \\ k1a & 0 & 0 & 0 & 0 & 0 & 0 & 0 & -(ka1+kab) & kba \\ 0 & 0 & 0 & 0 & 0 & k6b & 0 & 0 & kab & -(kba+kb6) \end{bmatrix} \begin{bmatrix} C_1 \\ C_2 \\ C_3 \\ C_4 \\ C_5 \\ C_6 \\ C_7 \\ C_8 \\ C_a \\ C_b \end{bmatrix} \tag{6}$$

individual partial reactions were isolated; i.e., (1) kinetic parameters for voltage-dependent reactions (Fig. 1, region I) were obtained from fitting the pre-steady-state currents in the absence of sugar (Loo et al. 2005) and (2) kinetic parameters for αMDG on the internal membrane surface (Fig. 1, region III) were obtained from our previous study on reverse sugar transport using the excised giant patch (Eskandari et al. 2005).

Simulations were performed by varying the rate constants (initially obtained by trial and error) until a global fit (by eye) was obtained for the experimentally obtained steady-state and pre-steady-state kinetics (steady-state I–V curves, $K_{0.5}^{Na}$, $K_{0.5}^{\alpha MDG}$, $K_{0.5}^{indican}$, time course of pre-steady-state currents, $Q-V$ and $\tau-V$ curves) and fluorescence intensity changes ($\Delta F-V$). The objective was to obtain a single set of parameters that fit the global data set rather than those required to obtain an optimal fit to one type of experiment. Each rate was varied in turn to determine the sensitivity of the simulations to that value.

The simulations shown in Figs. 2–4, 6, 7, 9 and 10 were carried out for hSGLT1 and TMR6M-labeled mutant G507C at 20°C using the parameters of Table 1 with $[Na^+]_o = 100$ mM, $[Na^+]_i = 5$ mM, $[\alpha MDG]_i = 0$ and $N_T \sim 10^{11}-10^{12}$ transporters. All simulations were performed at 0–100 mM $[Na^+]_o$, 0–10 mM $[\alpha MDG]_o$ and 0–10 mM $[indican]_o$.

Model Simulations

The kinetic parameters obtained for indican and αMDG are summarized in Table 1. Simulations with one set of parameters account for the steady-state and pre-steady-state kinetics of hSGLT1 in the presence of αMDG and/or indican. This is seen from the goodness of fit for the steady-state and pre-steady-state kinetics (e.g., Figs. 2D, E, 3B, 4D–F, 6D–F and 7D–F). The sensitivity of the fit was tested by systematically changing each parameter in turn; e.g., k_{27} and k_{72} can only be varied by threefold (keeping the ratio k_{72}/k_{27} constant) to account for the indican $K_{0.5}$ and the effect of indican on the time constants for the pre-steady-state currents. On the other hand, global fits are insensitive to variations in k_{85} from 100 to 1,000 s^{-1}: studies of outward currents as a function of internal [indican] are required to place limits on k_{85} (k_{58} is constrained by microscopic reversibility).

In order to account for the natural variation in kinetics from experiment to experiment, we determined the range in each parameter that is required (Table 1). The experimental parameters that vary include the following: (1) the $V_{0.5}$ for charge movement ($V_{0.5}^Q$) ranges from −33 to −70 mV (Loo et al. 2005), and this is accounted for by variation of k_{12} of 50,000–140,000 M^{-2}s^{-1} (Table 1); (2) the $K_{0.5}$ for indican is ∼60–100 μM, and this can be accounted for by

variations in k_{27} of ∼1000,000–300,000 M^{-1}s^{-1} and in k_{72} of ∼12–35 s^{-1}. As previously noted, there is a poor fit of the capacitive currents recorded in the submillisecond range, and this is probably due to our assumption about the simultaneous binding of the two external Na$^+$ ions to hSGLT1 (Loo et al. 2005).

The most striking differences between the kinetics of indican and glucose transport are in the turnover numbers, the competition between αMDG and indican and the effects of the sugars on the pre-steady-state kinetics. The fact that these differences can readily be accommodated may be taken as additional support for our model of Na$^+$/sugar cotransport by hSGLT1 (Fig. 8).

Specifically, the simulations permit the following:

1. *Isolation of conformation C$_7$Na$_2$S2*: Namely, undersaturating external Na$^+$ and indican concentrations at large negative membrane potentials, the transporter is predominantly in the C7Na$_2$S2 conformation ($P_o = 0.8$, Fig. 9B) due to the low rate of indican translocation ($k_{78} = 0.5$ s^{-1}). This is in sharp contrast to that for αMDG transport, where the transporter is predominantly in the C5Na$_2$ conformation ($P_o = 0.7$, Fig. 9C) due to the higher rate for sugar translocation ($k_{34} = 50$ s^{-1}) and low rate of Na$^+$ dissociation ($k_{56} = 5$ s^{-1}). The high population of state C7Na$_2$S2 in the presence of indican also accounts for (a) the charge transfer on depolarizing the membrane potential, i.e., the shift in conformation from C7Na$_2$S2 to C6 (C7Na$_2$S2 → C2Na$_2$ → C$_a$ → C$_b$ → C$_6$; Fig. 9B, E), and (b) the increase in time constant for both charge movement and fluorescence changes (Figs. 4 and 9). On the other hand, saturating αMDG eliminates charge movement—depolarizing the membrane potential shifts C5Na$_2$ to C$_6$ (Fig. 9C, F), an electroneutral step (see Loo et al. 2006). Implicit in the model is that the Na$^+$/sugar cotransport step (C3Na$_2$S1 → C4Na$_2$S1 and C7Na$_2$S2 → C8Na$_2$S2) is electroneutral and that the only voltage-sensitive steps in the transport cycle are those involving external Na$^+$ binding (C1 ⇌ C2Na$_2$) and the reorientation of the ligand-free transporter (C1 ⇌ C$_a$ ⇌ C$_b$ ⇌ C6, see Fig. 8).

2. *Evidence for a conformational change after sugar binding*: The conformational transitions monitored by fluorescence change (ΔF) when V_m is stepped from −50 mV (V_h) to + 50 mV differed in the presence of saturating concentrations of sugars: in saturating αMDG, ΔF is associated with transition from C5Na$_2$ → C6, whereas in saturating indican it arises from C7Na$_2$S2 → C6 (C7Na$_2$S2 → C2Na$_2$ → C1 → C$_a$ → C$_b$ → C6, Fig. 9B, C). The increase in maximal fluorescence change (ΔF_{max}) in saturating indican compared to NaCl buffer alone indicates that the (apparent) quantum yield of C7Na$_2$S2 is lower than

that of C2Na$_2$ ($qy_7 = 0.7$, $qy_2 = 1$). This difference in quantum yields between C2Na$_2$ and C7Na$_2$S2 provides evidence for a conformational change of SGLT1 induced by sugar binding, prior to the sugar translocation step.

3. *Substrate competition*: This is simply a consequence of the large difference in the transporter turnover number for the two substrates. In the case of SGLT1, where the turnover for indican is only 10% of that for αMDG, the addition of indican causes a reduction in αMDG transport. Simulations demonstrate that this is caused by an increase in the probability of the sugar-binding site being occupied by indican (see Fig. 10) and the concomitant reduction in translocation; k_{34} is reduced from 50 to 0.5 s^{-1} (k_{78}). The model accurately predicts the apparent inhibition constant for indican, 210 μM (Fig. 3), and the difference between this K_i and the $K_{0.5}$ for indican transport in the absence of other substrates (0.1 mM). Simulations also predict the changes in the kinetics of αMDG transport at fixed concentrations of indican; i.e., a fixed concentration of indican produces the expected decrease in apparent affinity (increase in $K_{0.5}$) of αMDG with no change in maximum velocity, or classical competitive inhibition. Irrespective of the fixed indican concentration, a sufficiently high αMDG concentration can be obtained, in theory at least, to outcompete indican binding.

References

Bezanilla F (2000) The voltage sensor in voltage-dependent ion channels. Physiol Rev 80:555–592

Birnir B, Loo DDF, Wright EM (1991) Voltage-clamp studies of the Na$^+$/glucose cotransporter cloned from rabbit small intestine. Pfluegers Arch 418:79–85

Briasoulis E, Judson I, Pavlidis N, Beale P, Wanders J, Groot Y, Veerman G, Schuessler M, Niebch G, Siamopoulos K, Tzamakou E, Rammou D, Wolf L, Walker R, Hanauske A (2000) Phase I trial of 6-hour infusion of glufosfamide, a new alkylating agent with potentially enhanced selectivity for tumors that overexpress transmembrane glucose transporters: a study of the European Organization for Research and Treatment of Cancer Early Clinical Studies Group. J Clin Oncol 18:3535–3544

Díez-Sampedro A, Lostao MP, Wright EM, Hirayama BA (2000) Glycoside binding and translocation in Na$^+$-dependent glucose cotransporters: comparison of SGLT1 and SGLT3. J Membr Biol 176:111–117

Díez-Sampedro A, Wright EM, Hirayama BA (2001) Residue 457 controls sugar binding and transport in the Na$^+$/glucose cotransporter. J Biol Chem 276:49188–49194

Eskandari S, Wright EM, Loo DDF (2005) Kinetics of the reverse mode of the Na$^+$/glucose cotransporter. J Membr Biol 204:23–32

Falk S, Guay A, Chenu C, Patil SD, Berteloot A (1998) Reduction of an eight-state mechanism of cotransport to a six-state model using a new computer program. Biophys J 74:816–830

Hazama A, Loo DDF, Wright EM (1997) Pre-steady-state currents of the Na$^+$/glucose cotransporter (SGLT1). J Membr Biol 155:175–186

Hirayama BA, Díez-Sampedro A, Wright EM (2001) Common mechanisms of inhibition for the Na$^+$/glucose (hSGLT1) and Na$^+$/Cl$^-$/GABA (hGAT1) cotransporters. Br J Pharmacol 134:484–495

Hirayama BA, Loo DDF, Díez-Sampedro A, Leung DW, Meinild A-K, Lai-Bing M, Turk E, Wright EM (2007) Na-dependent reorganization of the sugar-binding site of SGLT1. Biochemistry 46:13391–13406

Hirayama BA, Loo DDF, Wright EM (1997) Cation effects on protein conformations and transport in the Na$^+$/glucose cotransporter. J Biol Chem 272:2110–2115

Hirayama BA, Lostao MP, Panayotova-Heiermann M, Loo DDF, Wright EM (1996) Kinetic and specificity differences between rat, human and rabbit Na$^+$-glucose transporter (SGLT-1). Am J Physiol 270:G919–G926

King AE, Ackley MA, Cass CE, Young JD, Baldwin SA (2006) Nucleoside transporters: from scavengers to novel therapeutic targets. Trends Pharmacol Sci 27:416–425

Knutter I, Hartrodt B, Toth G, Keresztes A, Kottra G, Mrestani-Klaus C, Born I, Daniel H, Neubert K, Brandsch M (2007) Synthesis and characterization of a new and radiolabeled high-affinity substrate for H$^+$/peptide cotransporters. FEBS J 274:5905–5914

Larrayoz IM, Casado FJ, Pastor-Anglada M, Lostao MP (2004) Electrophysiological characterization of the human Na$^+$/nucleoside cotransporter 1 (hCNT1) and role of adenosine on hCNT1 function. J Biol Chem 279:8999–9007

Loewen SK, Yao SY, Slugoski MD, Mohabir NN, Turner RJ, Mackey JR, Weiner JH, Gallagher MP, Henderson PJ, Baldwin SA, Cass CE, Young JD (2004) Transport of physiological nucleosides and anti-viral and anti-neoplastic nucleoside drugs by recombinant *Escherichia coli* nucleoside-H$^+$ cotransporter (NupC) produced in *Xenopus laevis* oocytes. Mol Membr Biol 21:1–10

Loo DDF, Hazama A, Supplisson S, Turk E, Wright EM (1993) Relaxation kinetics of the Na$^+$/glucose cotransporter. Proc Natl Acad Sci USA 90:5767–5771

Loo DDF, Hirayama BA, Gallardo E, Lam J, Turk E, Wright EM (1998) Conformational changes couple Na$^+$ and glucose transport. Proc Natl Acad Sci USA 95:7789–7794

Loo DDF, Eskandari S, Hirayama BA, Wright EM (2002) A kinetic model for secondary active transport. In: Layton HE, Weinstein AM (eds), Membrane transport and renal physiology, the IMA volumes in mathematics and its applications, vol 129, Springer-Verlag, New York, pp 65–83

Loo DDF, Hirayama BA, Cha A, Bezanilla F, Wright EM (2005) Perturbation analysis of the voltage-sensitive conformational changes of the Na$^+$/glucose cotransporter. J Gen Physiol 125:13–36

Loo DDF, Hirayama BA, Karakossian MH, Meinild A-K, Wright EM (2006) Conformational dynamics of hSGLT1 during Na$^+$/glucose cotransport. J Gen Physiol 128:701–720

Loo DDF, Hirayama BA, Meinild A-K, Chandy G, Zeuthen T, Wright EM (1999) Passive water and ion transport by cotransporters. J Physiol 518:195–202

Lostao MP, Hirayama BA, Loo DDF, Wright EM (1994) Phenylglucosides and the Na$^+$/glucose cotransporter (SGLT1): analysis of interactions. J Membr Biol 142:161–170

Mackenzie B, Loo DDF, Wright EM (1998) Relationships between Na$^+$/glucose cotransporter (SGLT1) currents and fluxes. J Membr Biol 162:101–106

Mackey JR, Yao SYM, Smith KM, Karpinski E, Baldwin SA, Cass CE, Young JD (1999) Gemcitabine transport in *Xenopus* oocytes expressing recombinant plasma membrane mammalian nucleoside transporters. J Natl Cancer Inst 91:1876–1881

Meinild A-K, Hirayama BA, Wright EM, Loo DDF (2002) Fluorescence studies of ligand-induced conformational changes of the Na$^+$/glucose cotransporter. Biochemistry 41:1250–1258

Parent L, Supplisson S, Loo DDF, Wright EM (1992) Electrogenic properties of the cloned Na$^+$/glucose cotransporter: II. A transport model under nonrapid equilibrium conditions. J Membr Biol 125:63–79

Quick M, Loo DDF, Wright EM (2001) Neutralization of a conserved amino acid residue in the human Na$^+$/glucose transporter (hSGLT1) generates a glucose-gated H$^+$ channel. J Biol Chem 276:1728–1734

Sala-Rabanal M, Loo DDF, Hirayama BA, Turk E, Wright EM (2006) Molecular interactions between dipeptides, drugs and the human intestinal H$^+$-oligopeptide cotransporter hPEPT1. J Physiol 574:149–166

Sala-Rabanal M, Loo DDF, Hirayama BA, Wright EM (2008) Molecular mechanism of dipeptide and drug transport by the human renal H+/oliopeptide cotransporter, hPEPT2. Am J Physiol 294:F1422–F1432

Smith KM, Ng AML, Yao SYM, Labedz KA, Knaus EE, Wiebe LI, Cass CE, Baldwin SA, Chen X-Z, Karpinski E, Young JD (2004) Electrophysiological characterization of a recombinant human Na$^+$-coupled nucleoside transporter (hCNT1) produced in Xenopus oocytes. J Physiol 558:807–823

Veenstra M, Lanza S, Hirayama BA, Turk E, Wright EM (2004) Local conformational changes in the Vibrio Na$^+$/galactose cotransporter. Biochemistry 43:3620–3627

Veyhl M, Wagner K, Volk C, Gorboulev V, Baumgarten K, Weber WM, Schaper M, Bertram B, Wiessler M, Koepsell H (1998) Transport of the new chemotherapeutic agent beta-D-glucosyl-isophosphoramide mustard (D-19575) into tumour cells is mediated by the Na$^+$-D-glucose cotransporter SAAT1. Proc Natl Acad Sci USA 95:2914–2919

Yao SYM, Ng AML, Ritzel MWL, Gati WP, Cass CE, Young JD (1996) Transport of adenosine by recombinant purine- and pyrimidine-selective sodium/nucleoside cotransporters from rat jejunum expressed in Xenopus laevis oocytes. Mol Pharmacol 50:1529–1535

Zampighi GA, Kreman M, Boorer KJ, Loo DDF, Bezanilla F, Chandy G, Wright EM (1995) A method for determining the unitary functional capacity of cloned channels and transporters in Xenopus laevis oocytes. J Membr Biol 148:65–78